Structure

Multifaceted effects of N-glycosylation on amyloidogenic κ light chains in AL amyloidosis

--Manuscript Draft--

Manuscript Number:	STRUCTURE-D-25-00275R5
Full Title:	Multifaceted effects of N-glycosylation on amyloidogenic κ light chains in AL amyloidosis
Article Type:	Research Article
Keywords:	Antibody; Kappa-light chains; Systemic AL amyloidosis; N-glycosylation; Protein stability & dynamics; Protein secretion.
Corresponding Author:	Stefano Ricagno University of Milan Milano, ITALY
First Author:	Sarita Puri
Order of Authors:	Sarita Puri
	Valentina Speranzini
	Monica Russo
	Alice Nevone
	Uriel Petralia
	Manoj K. Sriramoju
	Yong-Sheng Wang
	Luca Broggini
	Giovanni Palladini
	Giampaolo Merlini
	Mario Nuvolone
	Shang-Te Danny Hsu
	Stefano Ricagno
Abstract:	Light chain amyloidosis (AL) is a fatal disorder caused by extracellular aggregation of monoclonal immunoglobulin light chains (LCs). While both λ and κ isotypes can be involved, κ-LCs account for only ~20% of cases, and their aggregation mechanisms remain less understood. Recent evidence suggests that N-glycosylation influences κ-LC aggregation and is strongly linked to AL amyloidosis. To investigate this, we examined patient-derived κ-LCs in both glycosylated and unglycosylated forms. Mass spectrometry confirmed the presence of complex-type N-glycans. Biophysical analyses showed that glycosylation enhances structural compactness, stabilizes the native structure, and promotes cooperative unfolding. Glycosylated κ-LCs also exhibited reduced conformational dynamics. Functionally, N-glycosylation significantly improved LC secretion efficiency and extracellular stability. These findings suggest that N-glycosylation acts as a protective factor against amyloid formation and enhances LC accumulation outside the cell. Overall, our study highlights the multifaceted and context-dependent role of N-glycosylation in modulating κ-LC behaviour, with important implications in AL pathogenesis.
Additional Information:	
Question	**Response**
Standardized datasets A list of datatypes considered standardized under Cell Press policy is	No

available here. Does this manuscript report new standardized datasets?	
Original code Does this manuscript report original computer code, algorithms, or computational models?	No

Dear Karin,

Thanks for accepting our manuscript for publication in Structure. We have edited the manuscript as per your suggestion and format required by your production team. We have not provided oligonucleotide sequences in the key resource table as none of the gene is cloned in our lab. They are rather synthesised by the Azenta Lifesciences company. We have included that information in the manuscript.

We thank you again for the time and efforts dedicated to the publication of this manuscript.

Best regards,

Stefano and Sarita

Editor's comments response

- The main document must include the following sections (in this order): title; author list and affiliations; Lead Contact footnote; email address(es) of corresponding author(s); Summary; Introduction; Results; Discussion; Resource Availability; Acknowledgments; Author Contributions; Declaration of Interests; main figure titles and legends; main tables and legends; STAR Methods text; supplemental video and Excel table titles and legends; and References.

  Response: We arrangement the manuscript in the above asked format. Our manuscript does not contain main text tables, so there is no section as main tables and legends. Rest of the handings are included as asked by editor.

- I suggest a minor edit for your title: "Multifaceted effects of N-glycosylation on amyloidogenic κ light chains in AL amyloidosis".
  Response: The title has been modified as editor's suggestion.

- We only allow a single Lead Contact. Please state only a single Lead Contact on the title page. (Multiple corresponding authors are fine.)
  Response: Only one lead contact is included in the manuscript i.e. Stefano Ricagno.

- Please remove the Highlights from the main manuscript word file. Instead please upload a single Word document that includes your Highlights and eTOC Blurb. Highlights are 3–4 bullet points of no more than **89 characters in length, including spaces**, and they summarize the core results of the paper in order to allow readers to quickly gain an understanding of the main take-home messages. **An eTOC blurb should also be included that is no longer than 50 words** describing the context and significance of the findings for the broader journal readership. When writing this paragraph, please target it to non-specialists by highlighting the major conceptual point of the paper in plain language, without extensive experimental detail. The blurb must be written in the third person and refer to "First Author et al."+
  Response: The highlights and eTOC have been provided in the above asked format and word limit is maintained strictly.

- Please show the subheadings in the main manuscript file in bold.
  Response: The subheadings of the manuscript are in bold now.

- Please provide the PRIDE accession code in the Data and Code Availability statement and key resources table.
  Response: PRIDE accession code has been provided in both Data and Code Availability statement and key resources table.

- Please provide all primer sequences used in your study and include them under "Oligonucleotides" in the key resources table. If there are more than 10 primer sequences, please show them in a suppl. table instead.

Response: All the plasmids used in this study are synthesised from Azenta life sciences and hence no oligonucleotides information is provided. We can provide whole plasmid details upon request to lead contact.

- You have included Tables 3-6 in the Suppl. Information file. Please note that we only allow a maximum of 10 main figures and tables. All main tables must be included before the STAR Methods section.
  Response: All the tables are part of supplemental files and hence renamed accordingly.

- All tables shown in the Suppl. Information file must be suppl. Tables.
  Response: All the tables are part of supplemental files and hence renamed accordingly.

- Please define the error bars and state the number of replicates in Figures 5 and 6.
  Response: The error bars and number of replicates are mentioned in the figures and figure legends, respectively.

Graphical abstract

Click here to access/download;Graphical Abstract;Graphical abstract_3.jpg

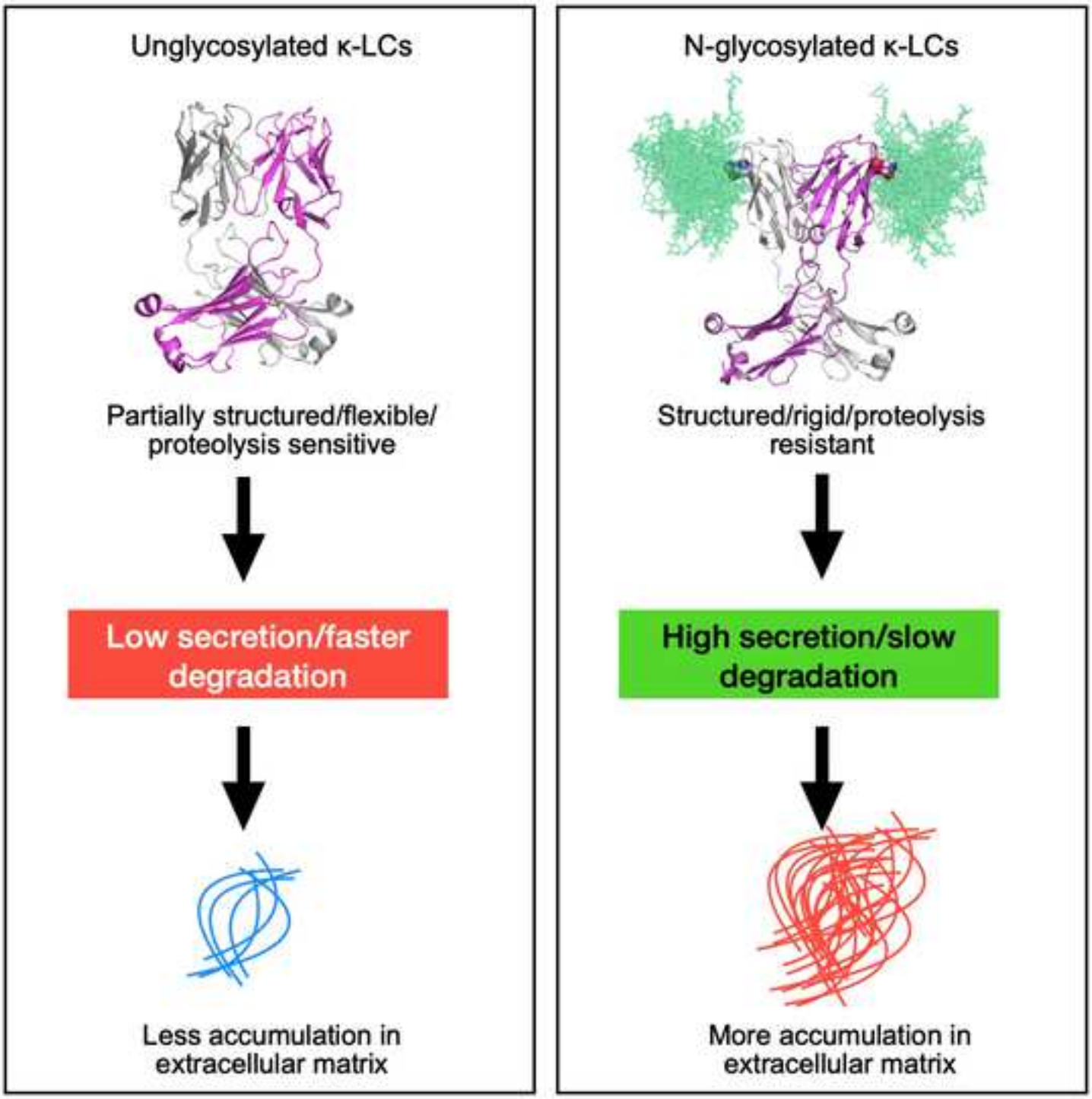

Multifaceted effects of N-glycosylation on amyloidogenic κ light chains in AL amyloidosis

Sarita Puri[1,2&], Valentina Speranzini[1], Monica Russo[3,4], Alice Nevone[3,4], Uriel Petralia[1], Manoj K. Sriramoju[5], Yong-Sheng Wang[5,6], Luca Broggini[1], Giovanni Palladini[3,4], Giampaolo Merlini[3,4], Mario Nuvolone[3,4], Shang-Te Danny Hsu[5,6,7], Stefano Ricagno[1,8&]

1. Department of Biosciences, University of Milan, Italy.
2. Biology Department, Indian Institute of Science Education and Research, Pune, India.
3. Department of Molecular Medicine, University of Pavia, Pavia, Italy.
4. Amyloidosis Research and Treatment Center, Fondazione IRCCS Policlinico San Matteo, Pavia, Italy.
5. Institute of Biological Chemistry, Academia Sinica, Taipei 11529, Taiwan.
6. Institute of Biochemical Sciences, National Taiwan University, Taipei 10617, Taiwan
7. International Institute for Sustainability with Knotted Chiral Meta Matter (WPI-SKCM[2]), Hiroshima University, 1-3-1 Kagamiyama, Higashi-Hiroshima, Hiroshima 739-8526, Japan.
8. Lead contact

& Corresponding to: Stefano.ricagno@unimi.it & saritapuri@iiserpune.ac.in

Summary

Light chain amyloidosis (AL) is a fatal disorder caused by extracellular aggregation of monoclonal immunoglobulin light chains (LCs). While both λ and κ isotypes can be involved, κ-LCs account for only ~20% of cases, and their aggregation mechanisms remain less understood. Recent evidence suggests that N-glycosylation influences κ-LC aggregation and is strongly linked to AL amyloidosis. To investigate this, we examined patient-derived κ-LCs in both glycosylated and unglycosylated forms. Mass spectrometry confirmed the presence of complex-type N-glycans. Biophysical analyses showed that glycosylation enhances structural compactness, stabilizes the native structure, and promotes cooperative unfolding. Glycosylated κ-LCs also exhibited reduced conformational dynamics. Functionally, N-glycosylation significantly improved LC secretion efficiency and extracellular stability. These findings suggest that N-glycosylation acts as a protective factor against amyloid formation and enhances LC accumulation outside the cell. Overall, our study highlights the multifaceted and context-dependent role of N-glycosylation in modulating κ-LC behaviour, with important implications in AL pathogenesis.

Introduction

Systemic immunoglobulin light chain (AL) amyloidosis is one of the most common systemic amyloid diseases characterized by the deposition of monoclonal immunoglobulin light chains (LCs) as amyloid fibrils in multiple organs, most critically

in the heart and kidneys.[1,2] Prefibrillar soluble species and deposition of fibrils in the heart significantly reduce the life span of patients; severe cardiac involvement results in an average survival time of approximately six months. These fibrils originate from overproduced immunoglobulin LCs secreted by a clonal plasma cell or B cell. Even though sequence patterns determining amyloid propensity remain to be identified, specific germline genes or gene families – particularly λ6 (*IGLV6*), λ1 (*IGLV1*), λ3 (*IGLV3*), and κ1 (*IGKV1*) – are significantly overrepresented in AL patients, suggesting that the starting germline sequences bear an intrinsic tendency to misfold and aggregate.[3-6] Given that the majority of LCs responsible for AL belong to the λ isotypes, the molecular properties determining their amyloidogenicity have been actively investigated. Amino acid sequence, structural heterogeneity, enhanced structural dynamics, higher unfolding rates, and reduced stability are considered the primary determinants of λ-LCs' aggregation propensity and soluble toxicity.[7-18]

Kappa LCs (κ-LCs) are typically less sensitive to aggregation due to their higher thermodynamic stability compared to λ-LCs, which may explain their under-representation in AL patients.[19,20] Still, approximately 20% of AL patients are linked to κ-LC aggregation.[20] The most common κ-germlines associated with AL amyloidosis are *IGKV1-33* and *IGKV1-39*. In particular, *IGKV1-33* encoded LCs show strong cardiac and renal tropism. Mutational analysis on *IGKV1-33* encoded LCs and other amyloidogenic germlines has shown that framework region 3 (FR3) and complementary determining region 3 (CDR3) of variable domain (VL) are most frequently mutated, with a large number of mutations in FR3.[6,21-23] Moreover, emerging evidence highlights the importance of post-translational modifications, especially N-glycosylation, in modulating κ-LC aggregation behaviour in AL patients.[22-29] Indeed, N-glycosylation, the enzymatic addition of complex oligosaccharides to the side-chain of asparagine residues within N-X-S/T sequon, is found in up to 40% of amyloidogenic κ-LCs in AL patients.[22-27] Nevone *et al*. demonstrated that N-glycosylation is statistically overrepresented in κ-LCs and that a specific glycosylation hotspot in FR3, where somatic mutations introduce an N-glycosylation sequon (NXT), leads to the overrepresentation of N-glycosylated κ-LCs in AL patients.[22]

Glycosylated κ-LCs are also a risk factor for Monoclonal Gammopathy of Undetermined Significance (MGUs) progressing to AL amyloidosis,[22] highlighting a clinical relevance and potential mechanistic role of N-glycosylation in LC aggregation and toxicity, which is not known to date. In addition, even though N-glycosylation does not seem to be statistically significant in λ-LCs, two *ex vivo* fibrils (PDB IDs 7NSL and 9FAA) formed by VL domains of λ-LCs display an N-glycosylation site, indicating that N-glycosylation is not protective against amyloid aggregation.[30,31] However, to date, the molecular consequences of N-glycosylation on LC structure, stability, dynamics, and secretion remain unexplored.

Thus, in this study, we examined the structural features, stability, and dynamics of three patient-derived N-glycosylated LCs belonging to κ1 and κ4 germlines, AC-LC1, AC-LC31, and AC-LC73, to gain insights into the role of N-glycosylation in amyloidogenic behaviour of κ-LCs associated with AL-amyloidosis. Moreover, the

secretion of these LCs in their glycosylated and unglycosylated forms and the impact of such secretions on cell metabolism were also assessed. The three AL patients, in whom these proteins were identified, showed cardiac infiltration with additional infiltration of AC-LC73 in the kidneys and liver. All three κ-LCs comprise one unique N-glycosylation sequon NFT located in the DE loop of the FR3 region, a N-glycosylation hot spot reported by Nevone *et al*.[22] N-glycosylated AC-LC1, AC-LC31, and AC-LC73 were over-expressed in Human embryonic kidney (HEK) Freestyle™ 293-F cells, while unglycosylated counterparts were over-expressed in *E. coli*. Our findings reveal that, in contrast to "pro-AL" mutations, which generally destabilize LCs and enhance aggregation, N-glycosylation contributes to structural compactness, enhances thermal and chemical stability, reduces fold dynamics, and enhances protease resistance. This is in line with the general role of N-glycosylation, which is known to stabilize protein folds.[32] Functionally, glycosylated κ-LCs exhibit increased secretion efficiency compared to their unglycosylated counterparts, a feature relevant for LC accumulation in the extracellular matrix (ECM) and its consequent aggregation and amyloid deposition in organs. Interestingly, in our study, this enhanced secretion of glycosylated κ-LCs was accompanied by reduced cell viability, suggesting that glycosylation either stabilizes cytotoxic species or results in a cellular secretion overload. Together, these results provide a comprehensive overview of how N-glycosylation modulates the conformational and functional landscape of κ-LCs, offering mechanistic insights into how post-translational modifications can drive or mitigate light chain pathology in AL amyloidosis.

Results

Sequence and clinical data

AC-LC1, AC-LC31, and AC-LC73 are patient-derived N-glycosylated clonal κ-LCs from three patients affected by systemic AL amyloidosis identified at the Amyloidosis Research and Treatment Center, University of Pavia, Italy.[22,33] AC-LC1 is encoded by the *IGKV1-33*-01, IGKJ1*01,* and *IGKC*01* gene segments, while AC-LC31 derives from *IGKV1-33*-01, IGKJ5*01,* and *IGKC*01*. In contrast, AC-LC73 is encoded by *IGKV4-1*01, IGKJ1*01,* and *IGKC*01*.[34] In terms of organ tropism, the AC-LC1 and AC-LC31 exhibit cardiac involvement, whereas AC-LC73 involves the heart, kidneys, and liver. A single N-glycosylation sequon (NFT) is present in the DE loop of the FR3 region of all three proteins.[22] Like all clonal LCs from patients with a monoclonal gammopathy, they have a significantly different VL domain, while a 100% conserved CL domain (Figure 1). To elucidate molecular determinants of amyloidogenic behaviour in N-glycosylated models, these proteins were overexpressed in HEK Freestyle™ 293-F cells, followed by His-tag-based affinity chromatography, thrombin-mediated His-tag removal, and final purification using size-exclusion chromatography (SEC). For comparison, the unglycosylated counterparts were recombinantly expressed and purified from host *E. coli*, as it lacks glycosylation machinery. The reason behind using *E. coli*-derived unglycosylated LCs is their sufficient yields upon purification when compared to unglycosylated LCs with QFT mutations expressed and secreted from HEK Freestyle™ 293-F cells. Both unglycosylated and N-glycosylated

AC-LC1 eluted as dimers (Figure S1A). In contrast, unglycosylated AC-LC31 exists in multiple oligomeric forms, suggesting its poor structural organization when compared to its N-glycosylated counterpart, which eluted as a well-defined single peak in the dimeric elution range (Figure S1B). The high degree of purity of the above variants is shown in Figure S2. These results are also in line with the secretion efficiency and stability of the QFT mutants of both proteins. Mutated AC-LC1 is more stable and more efficient in secretion compared to mutated AC-LC31 when expressed in HEK Freestyle™ 293-F cells (Figure S1 and Figures 6A and 6C), suggesting that the loss of N-glycosylation impacted AC-LC31 more than AC-LC1 (Figure S1, Figures 6A, and 6C). Moreover, the N-glycosylated form of AC-LC73 was also successfully purified; it exists as a stable dimer, with an SEC elution profile that overlaps with that of AC-LC1 (Figure S3). It exhibits a typical immunoglobulin fold, characterized by a far-UV CD minimum at 218 nm and a melting temperature of 47.5 ±0.6 °C, which is consistent with the values observed for N-glycosylated AC-LC1 and AC-LC31 (Figure S4). However, we were unable to purify unglycosylated AC-LC73 due to its poor refolding after inclusion body solubilisation, suggesting that N-glycosylation is important for the correct folding and stability of κ-LCs and imparts a differential level of protein stability on different LCs.

κ-LCs are properly glycosylated

N-glycosylation of the three κ-LCs expressed in HEK Freestyle™ 293-F cells was verified using PNGase F digestion and mass spectrometry (Figure 2). The shift towards a lower molecular weight band upon PNGase F digestion confirmed the glycan removal (Figure 2A), while mass spectrometry analysis revealed the presence of complex glycoforms decorated with N-Acetylglucosamine (GlcNAc). The single complex glycan HexNAc(5)Hex(4)Fuc(1)NeuAc(2) was predominant with a few minor variants in all three proteins (Figures 2B-2D). These findings align with *ex vivo* data, where monoclonal antibodies, Fc fusion proteins, and κ-LCs are known to carry complex glycoforms.[22,33]

Moreover, the overall yield of native unglycosylated κ-LCs was significantly lower than that of their glycosylated counterparts during protein purification; specifically, unglycosylated AC-LC73 displayed a very poor refolding yield. Thus, further experiments only focused on comparing the N-glycosylated and unglycosylated variants of AC-LC1 and AC-LC31.

N-glycosylation contributes to LCs' native structures

Far-UV circular dichroism (CD) and intrinsic fluorescence spectroscopies were employed to characterize the in-solution structural features of AC-LC1 and AC-LC31 in both their N-glycosylated and unglycosylated forms. Far-UV CD analysis revealed a β–sheet–rich immunoglobulin fold, as evidenced by a minimum at 218 nm (Figures 3A and 3C). In AC-LC1, the overlapping CD spectra for the N-glycosylated and unglycosylated forms (Figure 3A) indicated that the N-glycosylation does not alter the protein secondary structure. In contrast, the pronounced difference in the CD signal at

lower wavelengths near 200 nm for AC-LC31 (Figure 3C) suggested that the unglycosylated AC-LC31 has a slightly perturbed secondary structure.

Intrinsic fluorescence measurements of AC-LC1 demonstrated that the N-glycosylated form exhibited a 1.6-fold higher emission intensity compared to its unglycosylated counterpart, without any shift in the emission maximum (λ_{max}) (Figure 3B). This is likely due to reducing molecular rotation and non-radiative transitions in a compact structure, thereby increasing the quantum yield. Together, these findings suggest that N-glycosylation does not significantly alter the overall tertiary structure of AC-LC1 but instead reduces the flexibility of the VL domains, a region that is typically flexible in amyloidogenic light chains. In contrast, N-glycosylated AC-LC31 exhibited a 3.5-fold reduction in emission intensity accompanied by a blue shift of 14 nm, suggesting that its tryptophan residues are embedded in a well-folded, rigid protein core (Figure 3D). Of note, the difference in the intrinsic fluorescence behaviour for properly folded N-glycosylated AC-LC1 and AC-LC31 is likely due to the presence of an additional surface-exposed tryptophan residue, W96, in AC-LC1 (Figure S5). Together, these results highlight the crucial role of N-glycosylation in yielding the natively folded structures of these two κ-LCs.

N-glycosylation stabilises κ-LCs

To investigate the impact of N- glycosylation on the chemical and thermal stability of κ- LCs, we performed guanidinium chloride (GdnHCl)-mediated chemical unfolding and thermal denaturation experiments, respectively. First, the change in tertiary structure at increasing concentrations of GdnHCl (0–5.0 M) was monitored by measuring the intrinsic fluorescence emission in the range of 300 to 500 nm (Figures S6 and S7 (top panels)). Two- state fitting of singular-value decomposition (SVD) component (Figures S6 and S7 (bottom panels))[38,39] data revealed that both N-glycosylated AC-LC1 and AC-LC31 exhibit higher chemical stability than their unglycosylated counterparts, as evidenced by increased $[D]_{50\%}$ values (Figures 4A and 4C, Table S1). In addition, the unfolding curves for the N-glycosylated proteins showed a markedly higher resistance to denaturation at lower GdnHCl concentrations and a sharper transition, indicative of highly cooperative unfolding. The quantitative m-values (folding cooperativity) for N-glycosylated AC-LC1 and AC-LC31 were determined to be 6.4 ± 1.5 and 14.7 ± 5.5 kcal/mol/M, respectively, compared to 1.1 ± 0.2 and 7.2 ± 1.5 kcal/mol/M for their unglycosylated forms (Figures 4A and 4C). Overall folding stability of proteins is determined by both the midpoint of denaturation ($[D_{50}\ \%]$) and the folding cooperativity (m value); hence, the significantly higher m values and increased ($[D_{50}\ \%]$) result in a higher value for the glycosylated proteins (Table S1).

Thermal stability was assessed by monitoring the far-UV CD signal at 202 nm upon heating from 25 to 75 °C at a rate of 1 °C/min. All thermal denaturation profiles followed a two-state transition model. The apparent melting temperature (T_m) for N-glycosylated AC-LC1 was 47.3 ± 0.1 °C, 2.6 °C higher than that of its unglycosylated counterpart. Similarly, N- glycosylated AC-LC31 had a T_m of 45.0 ± 0.4 °C,

approximately 6 °C higher than its unglycosylated counterpart (Figure 4B and 4D). We also compared the extent of reversibility after complete denaturation of the unglycosylated and N-glycosylated proteins. We found that neither the unglycosylated nor the N-glycosylated proteins regained their native structures upon cooling, indicating irreversible unfolding (Figure S8). Together, chemical and thermal stabilities, and folding cooperativity indicate that N- glycosylation enhances the overall stability of native κ- LCs without affecting reversibility upon cooling.

Moreover, our data reveal a significant difference in the structural stability between the two N- glycosylated proteins, AC-LC1 and AC-LC31, even though they originate from the same germline gene (*IGKV1-33),* have an 89.3% sequence identity, share the same glycosylation type (complex type) and site (NFT sequon at position 70/71). This observation suggests that N-glycosylation contributes to their additional stabilization, but the specific amino acid sequence of each κ-LC remains its primary determinant.

N-glycosylation also provides rigidity to κ- LCs

To unravel the impact of N-glycosylation on the structural dynamics of κ-LCs, we performed trypsin-mediated limited proteolysis and hydrogen-deuterium exchange mass spectrometry (HDX-MS).

First, to directly compare the proteolytic sensitivity of N-glycosylated and unglycosylated k-LCs, we subjected the two variants of both proteins (AC-LC1, AC-LC31) to trypsin digestion at an enzyme-to-protein molar ratio of 1:100, monitoring full-length degradation over time (0–240 min) at 37°C. Interestingly, we observed that N-glycosylated κ-LCs exhibited a significantly slower digestion rate than their unglycosylated counterparts, indicating that N-glycosylation reduces protein flexibility, thereby reducing susceptibility to proteolytic cleavage (Figures 5A and 5C; Figure S9). To ensure that the enhanced sensitivity towards proteolysis was not simply due to N-glycosylation masking trypsin cleavage sites, we mapped the locations of lysine (Lys) and arginine (Arg) residues relative to the NFT sequon in the variable domain. Remarkably, our analysis revealed that the N-glycosylation site was spatially distant from trypsin cleavage sites in both LCs, confirming that the reduced proteolytic sensitivity arises from enhanced structural compactness rather than steric protection of the proteolytic sites by the glycosidic chain (Figure S10).

To investigate structural dynamics at the peptide level, we performed HDX-MS, a sensitive technique that probes protein flexibility by measuring the rate and extent of deuterium incorporation over time. To assess how N-glycosylation influences the dynamic properties of κ-LCs, we compared the HDX profiles of both unglycosylated and N-glycosylated forms of AC-LC1 and AC-LC31. This included analyzing (i) peptide-level relative H to D exchange within each protein (unglycosylated and glycosylated) and (ii) the differential H to D exchange of the common peptides between the unglycosylated LCs and their respective N-glycosylated counterparts under the same experimental conditions and exchange times. During the on-column pepsin digestion and subsequent data acquisition, back-exchange could occur, leading to underestimation of the actual deuterium uptake. Such an effect was not explicitly

corrected. Nonetheless, since all HDX-MS experiments were performed under identical experimental conditions using a fully automated liquid handling robotics, we focused on the relative deuterium uptakes, particularly for the pair-wise comparisons, assuming that the common peptides would experience the same degree of back-exchange under the same experimental conditions.

For individual protein analyses, we obtained excellent sequence coverage (>90%) for both AC-LC1 and AC-LC31 (Table S2, Figures S11, S13, S19, S21). The relative deuterium uptake of each protein over a time scale of 0–240 min is shown as heat maps (Figures S12, S14, S20, S22). The extent of relative deuterium uptake ranges from 0 to 30% relative to the zero-time point, and is shown on a gradient of blue to white to red (Figures S12, S14, S20, S22). Visual inspection of relative deuterium uptake in heat maps highlights that N-glycosylation does not reduce the deuterium uptake in AC-LC1, while it is quite significant for AC-LC31.

For the common-peptide comparisons, unglycosylated AC-LC1 and N-glycosylated AC-LC1 exhibited a sequence coverage of 76.3% with a redundancy of 4.04, while unglycosylated AC-LC31 and N-glycosylated AC-LC31 achieved 77.8% sequence coverage with a redundancy of 2.43 (Figures S15 and S23). The lower sequence coverage for the common-peptide sets was primarily due to the loss of peptides flanking the N-glycosylation site; the heterogeneity of glycoforms makes effective peptide searches challenging, even when post-translational modifications are considered. The relative deuterium uptake for the common peptides is presented as heat maps (ranging from 0 to 30% relative to the zero-time point) (Figures S16, S24). Details of the experiments, including the peptides identified, redundancy, peptide lengths, and average standard deviation in deuterium uptake, are provided in Table S2.

Pairwise comparison of deuterium uptakes using Dynamx, Deutero 2, and their mapping on AlphaFold predicted models of AC-LC1 and AL-CL31[40,41] revealed that N-glycosylation affects the structural dynamics of the two κ-light chains differently. For AC-LC1, both glycosylated and unglycosylated forms showed similar deuterium uptake throughout protein structure (Figures S17, S18, S27A, Figure 5B, Tables S3-S6). However, for AC-LC31, N-glycosylation led to noticeably reduced deuterium uptake across several areas, including the VL and CL domains (Figures S25, S26, S27B, Figure 5D, and Tables S7-S10). The most significant reduced deuterium uptake was seen in residues 5-12, 33-48 of the VL domain and residues 164-177 of the CL domain (Figures 5D, S25, and S26). The region specifically 33-48 for the VL-VL dimer interface and 164-177 form the VL-CL interface are crucial for providing structural rigidity to LCs as reported previously.[11] Examples of HDX differences after 10 minutes are shown in Figures 5B and 5D. Overall, these results show that N-glycosylation impacts deuterium uptake to varying degrees based on the specific κ-light chain. Moreover, this reduced uptake was observed not only near the glycosylation site (VL domain) but also farther away (CL domain), meaning that N-glycosylation stabilizes the whole protein structure. Despite the limited sample set, our findings indicate that N-glycosylation may generally stabilize κ-light chains, and the extent of stability is

dependent on individual LCs, as we see the most significant differences for AC-LC31 in all experiments, starting from the oligomerization states, in-solution structural features, thermal, chemical stabilities, trypsin digestion, and HDX-MS when compared to the AC-LC1 pair.

N-glycosylation enhances the secretion efficiency and reduces the metabolic activity of κ-LCs

In AL patients, LCs aggregation occurs in the extracellular space of multiple organs, such as the heart and kidneys[42], making secretion efficiency a critical step upstream of the aggregation process. To investigate the impact of N-glycosylation on LC extracellular secretion, we compared N-glycosylated κ-LCs with their unglycosylated counterparts (mutant with QFT sequon replacing NFT in wild-type). Both proteins (AC-LC1 and AC-LC31) were overexpressed in HEK Freestyle™ 293-F cells, and secretion was monitored via Western blot from day 0 to day 3 post-transfection (Figures 6A and 6C). These experiments aim to monitor the ability of unglycosylated LCs to fold in a cellular environment and to pass the quality checkpoints along the secretion pathway. Our results indicated that N-glycosylated LCs exhibit significantly higher secretion efficiency than their unglycosylated counterparts. Moreover, unglycosylated secreted proteins displayed multiple bands (Figure 6A), suggesting a higher degradation rate upon secretion.

Furthermore, we compared the metabolic activity of cells overexpressing N-glycosylated and unglycosylated proteins using a CellTiter-Glo luminescent cell viability assay. Interestingly, we found that the number of cells overexpressing glycosylated LCs is lower than that of their unglycosylated counterparts (Figures 6B and 6D). This observation suggests that the increased secretion and stability impose a higher cellular burden and hence impact the metabolic activity of cells. Together, our results suggest that N-glycosylation significantly enhances the extracellular secretion and stability of κ-LCs, but concomitantly, it reduces cell viability.

Discussion

In this study, we comprehensively analyzed the biophysical and functional consequences of N-glycosylation on two patient-derived kappa light chains (AC-LC1 and AC-LC31) associated with AL amyloidosis. Our results reveal that N-glycosylation enhances the structural compactness, stability, and rigidity of κ-LCs, thus exerting opposite effects compared to the destabilizing mutations typically observed in amyloidogenic LCs. A third κ-LC (AC-LC73) was native and stable when N-glycosylated, but it was excluded from the rest of this study because the unglycosylated variant could not be successfully refolded. Thus, even without a detailed characterisation, the different behaviour of the two AC-LC73 variants is in line with what was found for AC-LC1 and AC-LC31.

The enhanced structural compactness of AC-LC1 and AC-LC31, as observed via far-UV CD and intrinsic fluorescence measurements, suggests that glycan addition promotes native-like folding and structure assembly. This is particularly evident in AC-LC31, where unglycosylated variants exhibited altered secondary and tertiary

structure features indicative of misfolding or conformational heterogeneity. These observations align with the known role of glycosylation in improving folding efficiency and reducing conformational entropy in other protein systems.[43,44] Increased folding cooperativity, chemical, and thermal stabilities of glycosylated AC-LC1 and AC-LC31 further support the hypothesis that N-glycosylation contributes to conformational integrity. The higher midpoint denaturant concentrations ($[D]_{50\%}$), cooperativity (m-values), change in Gibbs free energies (ΔG_{NU}^{H2O}), and melting temperatures (T_m) also point to a stabilizing role of N-glycosylation that could maintain native conformation under physiological conditions. However, the unfolding of both unglycosylated and N-glycosylated LCs is irreversible, which might contribute to their aggregation once partial/complete unfolding occurs. The reduced proteolytic susceptibility and lower deuterium uptake in HDX-MS experiments further corroborate the idea that glycosylation imparts reduced backbone flexibility on the whole polypeptide, exerting short and long-range effects on the VL and CL domains, respectively. Interestingly, the protective effect was not due to steric masking of trypsin cleavage sites, but rather a consequence of globally reduced dynamics. All the above considerations point to a model where glycosylation-induced molecular effects should counteract the amyloidogenicity of AC-LC1 and AC-LC31 by favouring the native state over aggregation-prone conformers, thus mitigating early misfolding events. This is in stark contrast with the clinical data indicating that this N-glycosylation present in the FR3 region is significantly overrepresented in AL patients, and as such, it should be considered a molecular property facilitating AL onset.[22] Several considerations may contribute to explaining this apparent conundrum.

Even though glycan chains typically increase protein solubility and fold stability, glycosylation is present in several amyloid-forming proteins. In neurodegenerative diseases, various post-translational modifications, including O-glycosylation of α-synuclein, N-glycosylation of prion protein, and both N-glycosylation and phosphorylation of tau, are known to enhance the conformational stability of these proteins. Nevertheless, these modified protein species are abundantly found in the brains of patients with Parkinson's, Alzheimer's, and prion diseases, respectively, implicating these modifications in disease pathology.[45-50] Studies on tau aggregates have shown that the major fibrous components of neurofibrillary tangles, paired helical filaments (PHFs), require N-glycosylation for their typical morphology. Deglycosylation of tau has been reported to convert PHFs into straight filaments, which are thought to be involved in the early stages of insoluble neurofibrillary tangle (NFT) formation, thereby linking glycosylation status to tau filament architecture and aggregation behaviour.[46] More specifically, N-glycosylation has also been found in *ex vivo* amyloid formed by fragmented VL of λ-LCs, demonstrating that N-glycosylation is fully compatible with amyloid aggregation in AL patients.[30,31]

Interestingly, we observed that unglycosylated AC-LC1 and AC-LC31 are poorly secreted and are promptly degraded in the cell culture medium (Figure 6). This indicates that glycosylation may be crucial inside the cells to assist AC-LC1 and AC-LC31 folding and to stabilize their native state so that they can be ultimately secreted

and populated in the extracellular space.[51] Abundant and efficient secretion is instrumental in yielding the high concentration of circulating LCs, which is a necessary initial step for AL onset.[2] On the same line, N-glycosylation seems to render AC-LC1 and AC-LC31 more resilient to unspecific proteolysis, preventing immediate degradation upon protein secretion outside cells. Overall, these biophysical properties resemble those of stable non-amyloidogenic LCs associated with multiple myeloma, which typically do not aggregate even at high intracellular concentrations.[11,15] Nevertheless, counterintuitively, N-glycosylation of κ-LCs is selectively overrepresented in AL patients.[22] Thus, the contribution of N-glycosylation to disease may arise not only from efficient secretion. Several other roles for N-glycosylation can be suggested: altered interactions with extracellular matrix components, increasing local concentration or destabilising protein molecules; altered processing of N-glycosylated LCs in situ affecting the native fold, and such effects may result in subsequent aggregation. However, the experimental evaluation of these hypotheses is beyond the scope of this study: future *in vivo* aggregation studies, using either model organisms or 3D organoid systems that have a well-organized extracellular matrix, could help to fully establish the molecular roles of N-glycosylation in the aggregation of κ-LCs. A key limitation of this study is the use of *E. coli*–expressed, unglycosylated proteins for comparison with N-glycosylated light chains (LCs) produced in HEK Freestyle™ 293-F cells. Ideally, a more appropriate comparison would involve unglycosylated mutant variants expressed and purified from the HEK Freestyle™ 293-F cells to control for differences in post-translational processing and cellular context. However, this was not feasible in the present study due to markedly reduced secretion efficiency and increased susceptibility to degradation of the mutant proteins expressed and secreted from HEK Freestyle™ 293-F cells, which prevented their purification in sufficient quantities for comprehensive biochemical and biophysical analyses.

In summary, our data suggest that N-glycosylation, while stabilizing and protecting against intracellular misfolding, may in fact facilitate extracellular persistence, interactions, and accumulation, thereby contributing to disease pathology. These insights emphasize that stabilising protein modification may contribute to misfolding and aggregation and that post-translational modifications should be taken into account when evaluating the aggregation potential of κ-LCs. Finally, these data build a molecular rationale to explore potential therapeutic interventions that can modulate glycosylation pathways or counteract glycan-driven aggregation against AL amyloidosis.

Resource availability

Lead contact

Further information and requests for resources (plasmid and proteins), protocols, and reagents should be directed to and will be fulfilled by the lead contact Stefano Ricagno (stefano.ricagno@unimi.it).

Material availability

This study did not generate new unique reagents.

Data and code availability

- The NCBI accession code for AC-LC1, AC-LC31, and AC-LC73 are MZ595009.1 (Genebank USH96399.1), MZ595034.1 (GenBank: USH96424.1), MZ595076.1 (GenBank: USH96466.1), respectively.
- The HDX-MS data is submitted to PRIDE with an accession code PXD072495 and is publicly available as of the date of publication.
- This paper does not report original code.
- Other data reported in this paper will be shared by the lead contact upon request.
- Any additional information required to reanalyse the data reported in this paper is available from the lead contacts upon request.

Acknowledgments

This work was supported by the Italian Ministry of Research PRIN 2020 (20207XLJB2); by the Italian Ministry of Health (Ricerca Corrente and Ricerca Finalizzata, grant #GR-2018-12 368 387), by FONDAZIONE CARIPLO [grant number 2024-NAZ-0018 and 2023-1731]; by Fondazione CARIPLO/Telethon [Telethon GJC23044]; by Fondazione AIRC [IG 2024 ID 30307], by Università di Milano, Seed 4 Innovation 2024 grant to Nano-Detox. We acknowledge the access and services provided by the National Facility for Structural Biology, IU3 Biophysics Unit, Fondazione Human Technopole, Milan, Italy; Call for Access 25-SB-ROUND-1, Project ID2187057. SP acknowledges Fondazione Veronesi for a postdoctoral fellowship at the University of Milan, Italy, and DST Inspire faculty grant IFA23-LSBM 274 and the biology department, IISER Pune, India, for funding and infrastructure. STDH is supported by the Academia Sinica intramural fund, an Academia Sinica Investigator Award (AS-IV-114-L04) and an Infectious Disease Research Supporting Grant (AS-IDR-111-03 and AS-IDR-114-S01), and the National Science and Technology Council (NSTC), Taiwan (114-2123-M-001-008- and 113-2123-M-001-010). MKS is supported by the postdoctoral fellowships from the NSTC, Taiwan (113-2811-M-001-110 and 114-2811-M-001-116). Mass spectrometry data were acquired at the Academia Sinica Common Mass Spectrometry Facilities for Proteomics and Protein Modification Analysis located at the Institute of Biological Chemistry, Academia Sinica, supported by the Academia Sinica Core Facility and Innovative Instrument Project (AS-CFII-111-209).

Author contributions

Conceptualisation, S.P., S.R.; funding acquisition, S.P., S.-T.D., and S.R.; investigation, S.P., V.S., M.R., A.N., U.P., M.K.S., Y.-S.W., L.B.; resources, S.P., S.-T.D., M.N., G.V., S.R.; writing-original draft, S.P., S.R.; writing-review & editing, S.P., V.S., M.N., G.P., G.M., S.-T.D., and S.R.

Declaration of interests

The authors declare no competing interests.

Main figure titles and legends

Figure 1. Sequence and structural features of AC-LC1, AC-LC31, and AC-LC73. (A) Line representation of secondary structures, FRs, and CDRs, annotated with the corresponding amino acid sequence as defined by *Chothia and Lesk*.[35] (B) Multiple sequence alignment of the three κ-LCs, highlighting NFT sequon regions with a black dotted square. (C) GlycoSHIELD model of the N-glycosylated κ-LC. Cartoon representation of the dimeric AC-LC1 is shown in white and magenta for chain A and chain B, respectively. Green sticks represent the superposition of 30 frames of the 1 μs molecular dynamics simulation trajectory of a complex glycoform, Gal1_Fuc1, built in the GlycoSHIELD library[36]. The Asn71 residue is shown in a space-filled model with the carbon and nitrogen atoms colored in red and blue, respectively.

Figure 2: Characterisation of N-glycosylation of AC-LC1, AC-LC31, and AC-LC73. (A) PNGase F digestion confirms N-glycosylation of all three proteins. The lower bands highlighted with a star mark (*) represent the glycan-removed proteins, while the upper bands are the uncleaved proteins. (B) Mass spectrometry-based glycoproteomics analysis of the glycoforms in technical duplicates of AC-LC1, (C) AC-LC31, and (D) AC-LC73. The most abundant glycoforms are illustrated in the symbol nomenclature for glycans (SNFG).[37] Each histogram shows the relative abundance of different glycan structures detected at the N-glycosylation site for replicate 1 and replicate 2. The glycan structures identified in both replicates don't contain mannose and hence show the absence of high mannose and hybrid-type glycans. Instead, the N-glycosylation site predominantly carries complex-type glycans decorated with GlcNAC. A single complex glycan HexNAc(5)Hex(4)Fuc(1)NeuAc(2) (magenta color in all histograms) is predominant, with few minor variants shown with pink and dark magenta colors. The pie charts in each panel summarize the distribution of glycans at the N-glycosylation site within each replicate.

Figure 3: In-solution structural features of N-glycosylated and unglycosylated κ-LCs. (A-B) Far-UV CD and intrinsic fluorescence of N-glycosylated (green) and unglycosylated AC-LC1 (blue), respectively. (C-D) Far-UV CD and intrinsic fluorescence of N-glycosylated (green) and unglycosylated AC-LC31 (blue), respectively.

Figure 4: Thermal and chemical stability of N-glycosylated and unglycosylated κ-LCs. (A-B) Chemical and thermal unfolding transition curves of N-glycosylated AC-LC1 (green) and unglycosylated AC-LC1 (blue). (C-D) Chemical and thermal unfolding transition curves of AC-LC31. The colour code in all panels is the same as in panel A.

Figure 5: Dynamics of unglycosylated and N-glycosylated κ-LCs: (A) Limited proteolysis of N-glycosylated (green) and unglycosylated AC-LC1 (blue). The relative band intensity data are estimated from two independent replicates, and the standard deviation among them is shown as error bars. (B) Structural mapping of differential deuterium uptake between unglycosylated and N-glycosylated AC-LC1 after 10 min of HDX on a gradient of salmon to blue. The pink colour indicates similar or slightly higher

deuterium uptake in N-glycosylated proteins (-3%), and cyan indicates the same as the unglycosylated protein (0%). The NFT sequon is shown in red colour, while the covered region is shown in green colour. (C) Limited proteolysis of N-glycosylated (green) and unglycosylated AC-LC31 (blue). (D) Structural mapping of differential deuterium uptake between unglycosylated and N-glycosylated AC-LC31 after 10 min of HDX on a gradient of salmon (-6%), pink (-3%), cyan (0%), slate (3%), to blue (6%). N-glycosylated AC-LC31 showed overall greater protection than AC-LC1. All HDX-MS experiments were performed in three technical replicates. Error bars represent the standard deviation measured for each uptake time among three replicates.

Figure 6: Secretion and cell viability upon over-expression of N-glycosylated and unglycosylated κ-LCs. (A) Western blot showing secreted N-glycosylated and unglycosylated AC-LC1 at different days (0 to 3 days) of transfection. The upper arrow represents the full-length (FL) AC-LC1, while the lower one is the result of a partial degradation (PR) of AC-LC1. Western blot analyses were performed on two biological replicates, and one representative figure for each protein is shown as Panel A and Panel C. (B) Metabolic activity measurement upon over-expression of N-glycosylated (green) and unglycosylated (blue) AC-LC1. (C) Western blot showing secreted N-glycosylated and unglycosylated AC-LC31 at different days (0 to 3 days) of transfection. (D) Cell viability measurement upon over-expression of N-glycosylated (green) and unglycosylated (blue) AC-LC31. Cell viability assays were performed in two biological replicates, and the standard deviation between each measurement is shown as error bars.

STAR Methods

Key resources table

REAGENT or RESOURCE	SOURCE	IDENTIFIER
Antibodies		
Anti-histidine tag antibodies	Bio-Rad	MCA1396G
anti-mouse IgG conjugated to Horseradish Peroxidase (HRP)	Bio-Rad	1706516
Bacterial and virus strains		
E. coli DH5α	NEB® 5-alpha Competent *E. coli* (High Efficiency)	C2987H
BL21(DE3) Competent *E. coli*	NEB®	C2527H
Chemicals, peptides, and recombinant proteins		

FreeStyle 293 Expression Medium	Thermofisher Scientific Gibco	12338026 (6*1 liter)
Gibco™ GlutaMAX™-I	This paper	
293fectin™ Transfection Reagent, 1 mL	Thermofisher Scientific Gibco	12347019
Opti-MEM™ I Reduced Serum Medium, 100 mL	Thermofisher Scientific Gibco	31985062
Trypan Blue Solution, 0.4%	Thermofisher Scientific Gibco	15250061
Penicillin-Streptomycin mix	Sigma aldrich	P0781
Unglycosylated AC-LC1 pET21b + insert coding AC-LC1	This paper	N/A
Unglycosylated AC-LC31 pET21b + insert coding AC-LC1	This paper	N/A
N-glycosylated AC-LC1 pcDNA-3.1 +insert coding AC-LC1	This paper	N/A
N-glycosylated AC-LC31 pcDNA-3.1 +insert coding AC-LC31	This paper	N/A
N-glycosylated AC-LC73 pcDNA-3.1 +insert coding AC-LC73	This paper	N/A
Mutant AC-LC1 pcDNA-3.1 +insert containing CAG instead of AAC at position 274-276	This paper	N/A
Mutant AC-LC31 pcDNA-3.1 +insert containing CAG instead of AAT at position 280-282	This paper	N/A
Critical commercial assays		
CellTiter-Glo® luminescent assay	Promega	7570 (10 mL)
Deposited data		
HDX-MS data	This paper	PXD072495
Experimental models: Cell lines		

FreeStyle™ 293-F cells	Thermo Fisher Scientific	R79007
Recombinant DNA		
pET21b-AC-LC1 (Synthesized by Azenta Lifesciences)	This paper	N/A
pET21b-AC-LC31 (Synthesized by Azenta Lifesciences)	This paper	N/A
pcDNA-3.1 AC-LC1 (Synthesized by Azenta Lifesciences)	This paper	N/A
pcDNA-3.1 AC-LC31 (Synthesized by Azenta Lifesciences)	This paper	N/A
pcDNA-3.1 AC-LC73 (Synthesized by Azenta Lifesciences)	This paper	N/A
pcDNA-3.1 AC-LC1 mutant (Synthesized by Azenta Lifesciences)	This paper	N/A
pcDNA-3.1 AC-LC31 mutant (Synthesized by Azenta Lifesciences)	This paper	N/A
Software and algorithms		
PyMOL	Schrodinger LLC	http://www.pymol.org
Prism	Graphpad	http://www.graphpad.com/
PLGS	Waters	http://www.waters.com/
DynamX	Waters	http://www.waters.com/
GlycoSHIELD	Tsai et al.[36]	www.glycoshield.eu
Others		

HiPrep Q FF 16/10 (20 mL)	Cytiva	28936542
Superdex 75 10/300	Cytiva	29148721
Superdex 200 10/300	Cytiva	28990944

Experimental models and study participant details

Bacterial strains

DH5α (Cat. # C2987H) and BL21(DE3) (Cat. #C2527H) competent cells of *E. coli* were purchased from New England Biolabs. These strains were transformed with plasmid of our interests for plasmid amplification and unglycosylated LCs over-expression, respectively. They were grown at 37 ℃ and 180 rpm in an incubator shaker.

Cell lines

FreeStyle™ 293-F cells (Cat. #R79007) were purchased from Thermo Fischer Scientific and grown at 37 ℃ with 5% CO_2 for over expression and purification of N-glycosylated AC-LC1 and AC-LC31.

Method details

AC-LC1 structure prediction using glycoshield

Glycoshield (https://dioscuri-biophysics.pages.mpcdf.de/glycoshield-md/) is a web-based application that enables the grafting of glycan conformers onto specific amino acid residues in protein structures. To predict the glycosylated structure of AC-LC1, the AlphaFold-predicted model (used in the absence of an experimental structure)[40] was uploaded as the template. Both chains A and B were selected, along with residue N70, and a complex-type glycan (Gal1_Fuc1) was chosen to map on the model. Default parameters were used, including the CG grafting mode, a grafting cutoff of 3.5 Å, and multiple conformers of 30.[36,37] The resulting simulated structure was downloaded in PDB format and visualized with PyMOL (Figure 1).[52]

Protein expression and purification

N-glycosylated forms of AC-LC1, AC-LC31, and AC-LC73 were transiently expressed and secreted from HEK293 Freestyle™ cells cultured in suspension. For protein purification, one litre of clarified culture supernatant containing secreted protein was subjected directly to Ni-NTA affinity resin equilibrated with equilibration buffer containing 50 mM sodium phosphate and 200 mM NaCl (pH 8.0) for affinity-based chromatography. Eluted proteins in 300 mM imidazole-containing elution buffer were dialyzed overnight with simultaneous removal of the His-tag by thrombin cleavage (enzyme: protein ratio of 1:50). The tag-cleaved samples were re-applied to a Ni-NTA column, and the flow-through and wash fractions, containing the histidine-tag cleaved proteins, were collected. These were concentrated to 1 mL and further purified by SEC

for final polishing using 1x phosphate buffer saline (PBS: 10 mM Na_2HPO_4, 1.8 mM KH_2PO_4, 137 mM NaCl, 2.7 mM KCl) at pH 7.4. For the unglycosylated forms, all three proteins were expressed in *E. coli* and purified from inclusion bodies using a previously published protocol.[11,12] The inclusion bodies were solubilized in 6 M guanidine hydrochloride, followed by oxidative refolding using a redox buffer containing 20 mM Tris, 1 mM ethylenediaminetetraacetic acid (EDTA), 1 mM phenylmethylsulfonyl fluoride (PMSF), 5 mM reduced glutathione and 0.5 mM oxidized glutathione (pH 8.0) to facilitate disulfide bond formation. Refolded proteins were dialysed with 20 mM Tris (pH 8.0) for overnight to remove the access salt. The residual aggregated protein was removed by centrifugation followed by filtration. The filtered refolded protein was loaded on an anion exchange chromatography column (QFF 16/10) equilibrated with 20 mM Tris (pH 8.0). The final elution was collected using a buffer containing 20 mM Tris and 1 M NaCl (pH 8.0) gradient. The eluted peaks were collected and run on a 10% sodium-dodecyl sulphate polyacrylamide gel (SDS-PAGE). The fractions containing protein of our interest were pooled and concentrated to 10 mg protein to load on size-exclusion chromatography column (superdex 200 10/300) equilibrated in 1x phosphate buffer saline (PBS) buffer. The eluted proteins were again confirmed using SDS-PAGE and peak fractions containing pure protein were pooled (Figure S1-S2). Protein concentrations were determined by absorbance at 280 nm using the respective molar extinction coefficients: 28,670 $M^{-1} \cdot cm^{-1}$ for AC-LC1, 27,640 $M^{-1} \cdot cm^{-1}$ for AC-LC31, and 28,670 $M^{-1} \cdot cm^{-1}$ for AC-LC73. We were also successful in purifying correctly folded N-glycosylated AC-LC73 (Figures S3-S4). However, the refolding of unglycosylated AC-LC73 was poor, hence the low yield. For this reason, it was not included in further experiments. AC-LC1 and AC-LC31 protein stocks were aliquoted and stored at –20 °C for further use. Oligomerization status of purified proteins was confirmed by comparing their size-exclusion chromatography profiles using a superdex 200 10/300 increase column (Figures S1).

PNGase assay

The PNGase assay of the native N-glycosylated AC-LC1 and AC-LC31 proteins was performed according to *New England Biolabs* protocol (https://www.neb.com/en/protocols/pngase-f-protocol?srsltid=AfmBOopYsTHqFE_2UtLMjywU9FzExI9PV-iISsTNkcspUaCXBk1j9QO1). 10 µg of each protein, 2 µl of GlycoBuffer 2 (10X), and remaining MilliQ in a total reaction volume of 20 µl were incubated with 2 µl of PNGase F at 37 ℃ overnight. The reaction was terminated by incubating the reaction mixture in SDS-PAGE loading dye and heating at 95 ℃. The obtained samples were run on an SDS-PAGE gel to compare the migration of N-glycosylated and deglycosylated proteins.

In-solution structural features comparison between N-glycosylated and Unglycosylated κ-LCs

To assess and compare the secondary and tertiary structural features of N-glycosylated AC-LC1 and AC-LC31 with their unglycosylated counterparts, far-UV CD

and intrinsic fluorescence measurements were performed. All experiments were conducted at a protein concentration of 10 µM in 1x PBS at pH 7.4 and at a temperature of 25°C. Far-UV CD spectra were recorded in the wavelength range of 260–200 nm using a 1 mm path length quartz cuvette at a scan speed of 50 nm/min to evaluate secondary structure content. Intrinsic fluorescence emission spectra were collected upon excitation at 280 nm, with emission recorded from 300 to 500 nm. Both excitation and emission slit widths were set to 5 nm. The differences in emission intensity and shifts in emission maxima were used to compare the tertiary structures of the glycosylated versus unglycosylated forms of AC-LC1 and AC-LC31. The re-arrangement of all tryptophan residues in AC-LC1 and AC-LC31 are highlighted in AlphaFold model of both proteins with pink colour (Figure S5).

Chemical and thermal stability studies

To evaluate the impact of N-glycosylation on protein stability, the chemical and thermal stabilities of AC-LC1 and AC-LC31 were compared with their unglycosylated counterparts.

For chemical denaturation, purified proteins at a final concentration of 10 µM were incubated overnight with increasing concentrations of guanidine hydrochloride (GdnHCl), ranging from 0 to 5.0 M at 25°C, to allow equilibrium unfolding. Intrinsic fluorescence emission spectra were recorded from 300–500 nm upon excitation at 280 nm. Both excitation and emission slit widths were set to 5 nm. The resulting spectra were analyzed using SVD followed by data normalization (Figure S6, S7). Normalized fluorescence data were plotted as a function of GdnHCl concentration and fitted to a two-state unfolding model to determine the midpoint of denaturation ($[D]_{50}$ %), cooperativity (m-value), and change in ΔG_{NU}^{H2O} as described previously.[38,39,53,54] The obtained thermodynamic parameters were used to compare the chemical stability of glycosylated versus unglycosylated AC-LC1 and AC-LC31.

Thermal stability was assessed using far-UV CD spectroscopy. Proteins were subjected to a temperature ramp from 25 °C to 75 °C at a rate of 1 °C/min, and ellipticity was monitored at 202 nm and 218 nm. The resulting CD signals (in millidegrees) were normalized and plotted against respective temperatures. The thermal unfolding curves were fitted to a two-state model to determine the melting temperature (T_m) as described previously,[52,53] which was then compared between the glycosylated and unglycosylated forms of both proteins. To check the reversibility of the thermal unfolding process, the unfolding and refolding were followed by measuring the changes in the intrinsic fluorescence detected at both wavelengths of 350/330 nm using nano-Differential Scanning Fluorimetry (nanoDSF) (Prometheus, Nanotemper). Temperature ramps were performed in 1x PBS (pH 7.4) from 35°C to 90°C and from 90°C to 35 °C. Each experiment was performed in triplicate. The final protein concentration was 0.3 mg/ml. The reversibility of the thermal unfolding experiments was also checked by denaturing the proteins at 90°C and gradually reducing the temperature from 90 to 25°C (Figure S8).

Protein dynamics studies using limited proteolysis and hydrogen-deuterium exchange mass spectrometry

To compare the proteolytic susceptibility of N-glycosylated AC-LC1 and AC-LC31 with their unglycosylated counterparts, purified proteins were incubated with bovine trypsin at a 1:100 (enzyme: substrate) molar ratio. The reactions were carried out at a final protein concentration of 1 mg/mL in 50 mM sodium phosphate buffer containing 50 mM NaCl (pH 7.4), at 37 °C in a total volume of 250 µL. Aliquots of 20 µL were withdrawn at defined time points (0, 5, 10, 30, 60, 120, and 240 minutes) and immediately mixed with denaturing and reducing SDS-PAGE loading buffer. Samples were then heated at 95 °C for 20 minutes to terminate the proteolysis reaction (Figure S9). Digestion profiles were analyzed by SDS-PAGE, and the intensity of the intact (uncleaved) protein bands was quantified using ImageJ software. Band intensities were normalized with respect to the zero-minute time point and averaged from three independent replicates. The obtained digestion profiles are not a result of masking of trypsin digestion sites by N-glycosylation as they are equally accessible in N-glycosylated and unglycosylated variants (Figure S10). The relative intensities were plotted against time to assess and compare the kinetics of proteolytic degradation for the glycosylated and unglycosylated forms of AC-LC1 and AC-LC31, as described previously.[12]

HDX-MS experiments were performed in fully automated mode using a SYNAPT G2-HDMS mass spectrometer coupled with a LEAP robotic liquid handling system (Waters Corporation, USA) as described previously.[54-57] N-glycosylated and unglycosylated model proteins were prepared at an initial concentration of 80 µM and diluted 20-fold into labelling buffer (5 mM potassium phosphate, pD 7.0 in D_2O) to initiate HDX. Exchange reactions were carried out at 25 °C for 0, 0.5, 1, 10, 30, 120, and 240 minutes in technical triplicate. At each time point, samples were quenched by 1:1 mixing with ice-cold quench buffer (50 mM potassium phosphate, pH 2.3 in H_2O). Online digestion was performed at 15 °C using an immobilized pepsin column (Waters Enzymes BEH Pepsin, 2.1 × 30 mm), followed by peptide trapping on a C18 trapping column (Acquity BEH VanGuard, 1.7 µm, 2.1 × 5.0 mm). Peptide separation was achieved using a linear acetonitrile gradient from 5% to 40%. Mass spectra were acquired using lock mass calibration with (Glu^1)-fibrinopeptide B (CAS No. 103213-49-6, Merck, USA; expected m/z: 785.8426 Da). Data processing was performed using ProteinLynx Global Server (PLGS) and DynamX software (Waters Corporation, USA). Peptides identified at zero exchange time using PLGS were imported into DynamX along with raw data from all time points. Peptide filtering criteria in DynamX included: a file threshold of 3, minimum intensity of 1000, minimum product ions per amino acid of 0.1, and a maximum MH^+ error of 5 ppm. Relative deuterium uptake for individual peptides and differential uptake between glycosylated and unglycosylated forms were quantified. Heatmaps representing deuterium incorporation per residue were generated and mapped onto monomeric models using PyMOL (Schrödinger, USA) for structural visualization (Figures S11-S27).[52]

In addition to Dynmax, the statistical significance of our differential deuterium uptake between the unglycosylated and N-glycosylated LCs was determined using an online available software Deutero 2.[41] The input files for the deuterons were HDX differential uptake cluster data obtained from the Dynamx analysis. The software shortlists common peptides that have accepted errors for individual exchange time points. The obtained statistics show the estimate of differential uptake, standard error between the estimates, t-significance, and p-values. A significant score of ≥98% is considered significant (Tables S3-S10, Figures S18, S26).

Measurements of protein secretion efficiencies and metabolic activity

N-glycosylation is a well-characterized post-translational modification known to enhance protein secretion and modulate cellular homeostasis.[43] Given that extracellular aggregation is a hallmark of amyloidogenic light chains (LCs), efficient secretion into the extracellular space is a prerequisite for their pathogenic behavior. To investigate the effect of disease-associated N-glycosylation on secretion efficiency, both N-glycosylated and unglycosylated counterparts of AC-LC1 and AC-LC31, where the NFT sequon is mutated to QFT, were transiently overexpressed in HEK293 Freestyle™ cells at 37 °C, 5% CO_2, and 150 rpm shaking. Secretion kinetics were monitored over a 3-day time course post-transfection (days 0, 1, 2, and 3). All experiments were performed in two biological replicates. An equal amount of supernatant normalized with respect to the number of cells was collected at each time point and analyzed by SDS-PAGE, followed by immunoblotting using anti-His-tag antibodies to detect the overexpressed proteins specifically. Secretion levels were compared by visual inspection of band intensities between the N-glycosylated and unglycosylated proteins. Metabolic activity under each experimental condition was also assessed using the CellTiter-Glo® luminescent assay (Promega), which measures ATP levels as a proxy for metabolically active cells. The secretion and viability assays were independently performed for both AC-LC1 and AC-LC31, allowing direct comparison between their glycosylated and unglycosylated forms.

Quantification and statistical analysis

The corresponding quantification and statistics for each experiment is given in the methods and figure legends section of each figure.

References

1. Merlini, G., Dispenzieri, A., Sanchorawala, V., Schönland, S.O., Palladini, G., et al. (2018). Systemic immunoglobulin light chain amyloidosis. Nat. Rev. Dis. Primers 4, 38.
2. Sanchorawala, V. (2024). Systemic Light Chain Amyloidosis. N. Engl. J. Med 390, 2295–2307.
3. Enqvist, S., Sletten, K., Stevens, F. J., Hellman, U., and Westermark, P. (2007). Germ-line origin and somatic mutations determine the target tissues in systemic AL-Amyloidosis. PLoS One 2, e981

4. Comenzo, R. L., Wally, J., Kica, G., Murray, J., Ericsson, T., Skinner, M., and Zhang, Y. (1999). Clonal immunoglobulin light chain variable region germline gene use in AL amyloidosis: association with dominant amyloid- related organ involvement and survival after stem cell transplantation. Br. J. Haematol 106, 744–751
5. Perfetti, V., Palladini, G., Casarini, S., Navazza, V., Rognoni, P., Obici, L., et al. (2012). The repertoire of λ light chains causes predominant amyloid heart involvement and identification of a preferentially involved germline gene, IGLV1-44. Blood 119, 144-150
6. Puri, S., Chaudhary, I., Khatri, A., Patel, B., Kumawat, A., Palkar, S., et al. (2025). The conformational landscape of AlphaFold2 - predicted amyloidogenic light chains and their correlation with VL domain mutations and aggregation propensity. J Mol. Recognition 38, e70011.
7. Peterson, F. C., Baden, E. M., Owen, B. A. L., Volkman, B. F., and Ramirez-Alvarado, M. (2010). A single mutation promotes amyloidogenicity through a highly promiscuous dimer interface. Structure 18, 563–570
8. Baden, E. M., Owen, B. A. L., Peterson, F. C., Volkman, B. F., Ramirez-Alvarado, M., and Thompson, J. R. (2008). Altered dimer interface decreases stability in an amyloidogenic protein. *J.* Biol. Chem 283, 15853–15860
9. Rottenaicher, G. J., Weber, B., Rührnößl, F., Kazman, P., Absmeier, R. M., et al. (2021). Molecular mechanism of amyloidogenic mutations in hypervariable regions of antibody light chains. J. Biol. Chem. 296, 100334
10. Rottenaicher, G. J., Absmeier, R. M., Meier, L., Zacharias, M. and Buchner, J. (2023). A constant domain mutation in a patient-derived antibody light chain reveals principles of AL amyloidosis. Commun Biol. 6, 209
11. Paissoni, C., Puri, S., Broggini, L., Sriramoju, M. K., Maritan, M., Russo, R., Speranzini, V. et al. (2025). A conformational fingerprint for amyloidogenic light chains. eLife 10.7554/eLife.102002.2
12. Puri, S., Gadda, A., Polsinelli, I., Barzago, M. M., Toto, A., Sriramoju, M. K., et al. (2025). The critical role of the variable domain in driving proteotoxicity and aggregation in full-length light chains. J. Mol. Biol. 437, 168958
13. Rennella, E., Morgan, G. J., Kelly, J. W., and Kay, L. E. (2019). Role of domain interactions in the aggregation of full-length immunoglobulin light chains. Proc. Natl. Acad. Sci. U.S.A. 116, 854–863
14. Lavatelli, F., Natalello, A., Marchese, L., Ami, D., Corazza, A., Raimondi, S., Mimmi, M. C., Malinverni, S., Mangione, P. P., Palmer, M. T., Lampis, A., Concardi, M., Verona, G., Canetti, D., Arbustini, E., Bellotti, V., and Giorgetti, S. (2024). Truncation of the constant domain drives amyloid formation by immunoglobulin light chains. J. Biol. Chem. 300, 107174
15. Oberti, L., Rognoni, P., Barbiroli, A., Lavatelli, F., Russo, R., Maritan, M., Palladini, G., Bolognesi, M., Merlini, G., and Ricagno, S. (2017). Concurrent structural and biophysical traits link with immunoglobulin light chains amyloid propensity. Sci Rep. 7, 16809

16. Weber, B., Hora, M., Kazman, P., Göbl, C., Camilloni, C., Reif, B., and Buchner, J. (2018). The antibody light-chain linker regulates domain orientation and amyloidogenicity. J. Mol. Biol. 430, 4925–4940
17. Absmeier, R. M., Rottenaicher, G. J., Svilenov, H. L., Kazman, P., and Buchner, J. (2023). Antibodies gone bad – the molecular mechanism of light chain amyloidosis. The FEBS Journal 290, 1398–1419
18. Puri, S., Palkar, S., Kumawat, A., Chaudhary, I., Patel, B., et al. (2025). Dimer dissociation and aggregation hot-spot exposure synergistically accelerate light chain variable domain aggregation associated with AL amyloidosis. J. Mol. Biol. *437*(24), 169468.
19. Blancas-Mejía, L. M., Misra, P., and Ramirez-Alvarado, M. (2017). Differences in protein concentration dependence for nucleation and elongation in light chain amyloid formation. Biochemistry 56, 757–766
20. Blancas-Mejía, L. M., and Ramirez-Alvarado, M. (2016). Recruitment of light chains by homologous and heterologous fibrils shows distinctive kinetic and conformational specificity. Biochemistry 55, 2967–2978
21. Schreiner, S., Berghaus, N., Poos, A. M., Raab, M. S., Besemer, B., Fenk, R., Goldschmidt, H., Mai, E. K., Müller-Tidow, C., Weinhold, N., Hegenbart, U., Huhn, S., and Schönland, S. O. (2024). Sequence diversity of kappa light chains from patients with AL amyloidosis and multiple myeloma. Amyloid 31, 86–94
22. Nevone, A., Girelli, M., Mangiacavalli, S., Paiva, B., Milani, P., Cascino, P., et al. (2022). An N-glycosylation hotspot in immunoglobulin κ light chains is associated with AL amyloidosis. Leukemia 36, 2076–2085
23. Mellors, P. W., Dasari, S., Kohlhagen, M. C., Kourelis, T., Go, R. S., Muchtar, E., et al. (2021). MASS-FIX for the detection of monoclonal proteins and light chain N-glycosylation in routine clinical practice: a cross-sectional study of 6315 patients. Blood Cancer J. 11, 50
24. Kumar, S., Dispenzieri, A., Dasari, S., Milani, P., Merlini, G., Hetrick, M., Barnidge, D., Madden, B., and Murray, D. (2018). Mass spectrometric approach to identify N-glycosylation of light chain in patients with immunoglobulin light chain amyloidosis (AL). Cancer Research 78, 2693–2693
25. Kumar, S., Murray, D., Dasari, S., Milani, P., Barnidge, D., Madden, B., et al. (2019). Assay to rapidly screen for immunoglobulin light chain glycosylation: a potential path to earlier AL diagnosis for a subset of patients. Leukemia 33, 254–257
26. Dispenzieri, A., Larson, D. R., Rajkumar, S. V., Kyle, R. A., Kumar, S. K., Kourelis, T., Arendt, B., Willrich, M., Dasari, S., and Murray, D. (2020). N-glycosylation of monoclonal light chains on routine MASS-FIX testing is a risk factor for MGUS progression. Leukemia 34, 2749–2753
27. Milani, P., Murray, D. L., Barnidge, D. R., Kohlhagen, M. C., Mills, J. R., Merlini, G., Dasari, S., and Dispenzieri, A. (2017). The utility of MASS- FIX to detect and monitor monoclonal proteins in the clinic. American J Hematol. 92, 772–779

28. Steven, F. J., Kislevsky, R. (2000). Immunoglobulin light chains, glycosaminoglycans, and amyloid. Cell Mol Life Sci. 57(3), 441-449.
29. Omtvedt, L. A., Bailey, D., Renouf, D. V., Davies, M. J., Paramonov, N. A., Haavik, S., Husby, G., Sletten, K., Hounsell, E. F. (2000). Glycosylation of immuoglobulin light chains associated with AL amyloidosis. Amyloid 7(4).
30. Radamaker, L., Karimi-Farsijani, S., Andreotti, G., Baur, J., Neumann, M., Schreiner, S., Berghaus, N., Motika, R., Haupt, C., Walther, P., Schmidt, V., Huhn, S., Hegenbart, U., Schönland, S. O., Wiese, S., Read, C., Schmidt, M., and Fändrich, M. (2021). Role of mutations and post-translational modifications in systemic AL amyloidosis studied by cryo-EM. Nat Commun. 12, 6434
31. Schulte, T., Chaves-Sanjuan, A., Speranzini, V., Sicking, K., Milazzo, M., Mazzini, G., Rognoni, P., Caminito, S., Milani, P., Marabelli, C., Corbelli, A., Diomede, L., Fiordaliso, F., Anastasia, L., Pappone, C., Merlini, G., Bolognesi, M., Nuvolone, M., Fernández-Busnadiego, R., Palladini, G., and Ricagno, S. (2024). Helical superstructures between amyloid and collagen in cardiac fibrils from a patient with AL amyloidosis. Nat Commun. 15, 6359
32. Higel, F., Seidl, A., Sörgel, F., and Friess, W. (2016). N-glycosylation heterogeneity and the influence on structure, function, and pharmacokinetics of monoclonal antibodies and Fc fusion proteins. European Journal of Pharmaceutics and Biopharmaceutics 100, 94-100
33. Cascino, P., Nevone, A., Piscitelli, M., Scopelliti, C., Girelli, M., Mazzini, G., Caminito, S., Russo, G., Milani, P., Basset, M., et al. (2022). Single-molecule real-time sequencing of the M protein: Toward personalized medicine in monoclonal gammopathies. Am J Hematol. 97, E389–E392.
34. Manso, T., Folch, G., Giudicelli, V., Jabado-Michaloud, J., Kushwaha, A., et al. (2022). IMGT® databases, related tools, and web resources through three main axes of research and development. Nucleic Acid Research 50(D1), D1262-72.
35. Al-Lazikani, B., Lesk, A. M., Chothia, C. (1997). Standard conformations for the canonical structures of immunoglobulins. J. Mol. Biol. 273, 927–948
36. Tsai, Y.-X., Chang, N.-E., Reuter, K., Chang, H.-T., Yang, T.-J., Von Bülow, S., Sikora, M., et al. (2024). Rapid simulation of glycoprotein structures by grafting and steric exclusion of glycan conformer libraries. Cell 187(5), 1296-1311.e26.
37. Varki, A., Cummings, R. D., Aebi, M., Packer, N. H., Seeberger, P. H., Esko, J. D. et al. (2015). Symbol nomenclature for graphical representations of glycans. Glycobiology 25, 1323–24.
38. Wang, I., Chen, S.-Y., and Hsu, S.-T.D. (2015). Unraveling the folding mechanism of the smallest knotted protein, MJ0366. J. Phys. Chem. B. 119, 4359–4370.
39. Wang, I., Chen, S.Y., & Hsu, S.-T. D. (2016). Folding analysis of the most complex Stevedore's protein knot. Sci Rep. 6, 31514.
40. Jumper, J., Evans, R., Pritzel, A., Green, T., Figurnov, M., Ronneberger, O., Tunyasuvunakool, K., Bates, R., Žídek, A., Potapenko, A., et al. (2021). Highly accurate protein structure prediction with AlphaFold. Nature 596, 583–589

41. Lau, A. M., Claesen, J., Hansen, K., Politis, A. (2021). Deuteros 2.0: peptide-level significance testing of data from hydrogen-deuterium exchange mass spectrometry. Bioinformatics 37(2), 270-272.
42. Buxbaum, J. (2003). Diseases of protein conformation: what do in vitro experiments tell us about in vivo diseases? Trends in Biochemical Sciences 28, 585–592
43. Hoffmann, D., and Flörke, H. (1998). A structural role for glycosylation: lessons from the hp model. Folding and Design 3, 337–343
44. Hao, C., Zou, Q., Bai, X., and Shi, W. (2025). Effect of glycosylation on protein folding: From biological roles to chemical protein synthesis. iScience 28, 112605
45. Farzadfard, A., König, A., Petersen, S.V., Nielsen, J. et al. (2022). Glycation modulates alpha-synuclein fibrillization kinetics: A sweet spot for inhibition. J. Biol. Chem. 298, 101848.
46. Takahashi, M., Tsujioka, Y., Yamada, Y. T. et al. (1999). Liposits, Glycosylation of microtubule-associated protein tau in Alzheimer's disease brain. Acta Neuropathologica 97, 635-641.
47. Cancellotti, E., Mahal, S.P., Somerville, R., Diack, A., Brown, D., Piccardo, P., Weissmann, C., and Manson, J. C. (2013). Post-translational changes to PrP alter transmissible spongiform encephalopathy strain properties. EMBO J. 32, 756–769.
48. Katorcha, E., Makarava, N., Savtchenko, R., d′Azzo, A., and Baskakov, I. V. (2014). Sialylation of prion protein controls the rate of prion amplification, the cross-species barrier, the ratio of PrPSc glycoform and prion infectivity. PLoS Pathogen 10, e1004366.
49. Mishra, R., Elgland, M., Begum, A., Fyrner, T., Konradsson, P., Nyström, S., and Hammarström, P. (2019). Impact of N-glycosylation site variants during human PrP aggregation and fibril nucleation. BBA - Proteins & Proteomics 1867, 909–921.
50. Schilling, K.M., Jorwal, P., Ubilla-Rodriguez, N.C., Assafa, T.E., Gatdula, J.R.P., Vultaggio, J.S., Harris, D.A., and Millhauser, G.L. (2023). N-glycosylation is a potent regulator of prion protein neurotoxicity. J. Biol. Chem. 299,105101.
51. Benham, A. M. (2012). Protein secretion and the endoplasmic reticulum. Cold Spring Harbor Perspectives in Biology, a012872–a012872
52. Schrödinger, LLC & DeLano, W. *PyMOL*. Retrieved from http://www.pymol.org/pymol
53. Puri, S., and Hsu, S.-T. D. (2022) Elucidation of folding pathways of knotted proteins. in Methods in Enzymology, Elsevier 675, 275–297
54. Puri, S., Liu, C.-Y., Hu, I.-C., Lai, C.-H., Hsu, S.-T. D., and Lyu, P.-C. (2023). Elucidation of the folding pathway of a circular permutant of topologically knotted YbeA by tryptophan substitutions. Biochem. Biophy. Res. Commun. 672, 81–88

55. Puri, S., Chen, S.-N., Chiu, Y.-H., Draczkowski, P., Ko, K.-T., Yang, T.-J., Wang, Y.-S., Uchiyama, S., and Hsu, S.-T. D. (2022). Impacts of cancer-associated mutations on the structure–activity relationship of BAP1. J. Mol. Biol. 434, 167553
56. Puri, S., and Hsu, S.-T. D. (2021). Cross-over loop cysteine C152 acts as an antioxidant to maintain the folding stability and deubiquitinase activity of UCH-L1 under oxidative stress. J. Mol. Biol. 433, 166879
57. Sun, C.-P., Chiu, C.-W., Wu, P.-Y., Tsung, S.-I., Lee, I.-J., Hu, C.-W., Hsu, M.-F., Kuo, T.-J., Lan, Y.-H., Chen, L.-Y., et al. (2023). Development of AAV-delivered broadly neutralizing anti-human ACE2 antibodies against SARS-CoV-2 variants. Molecular Therapy 31, 3322–3336

Figure 1

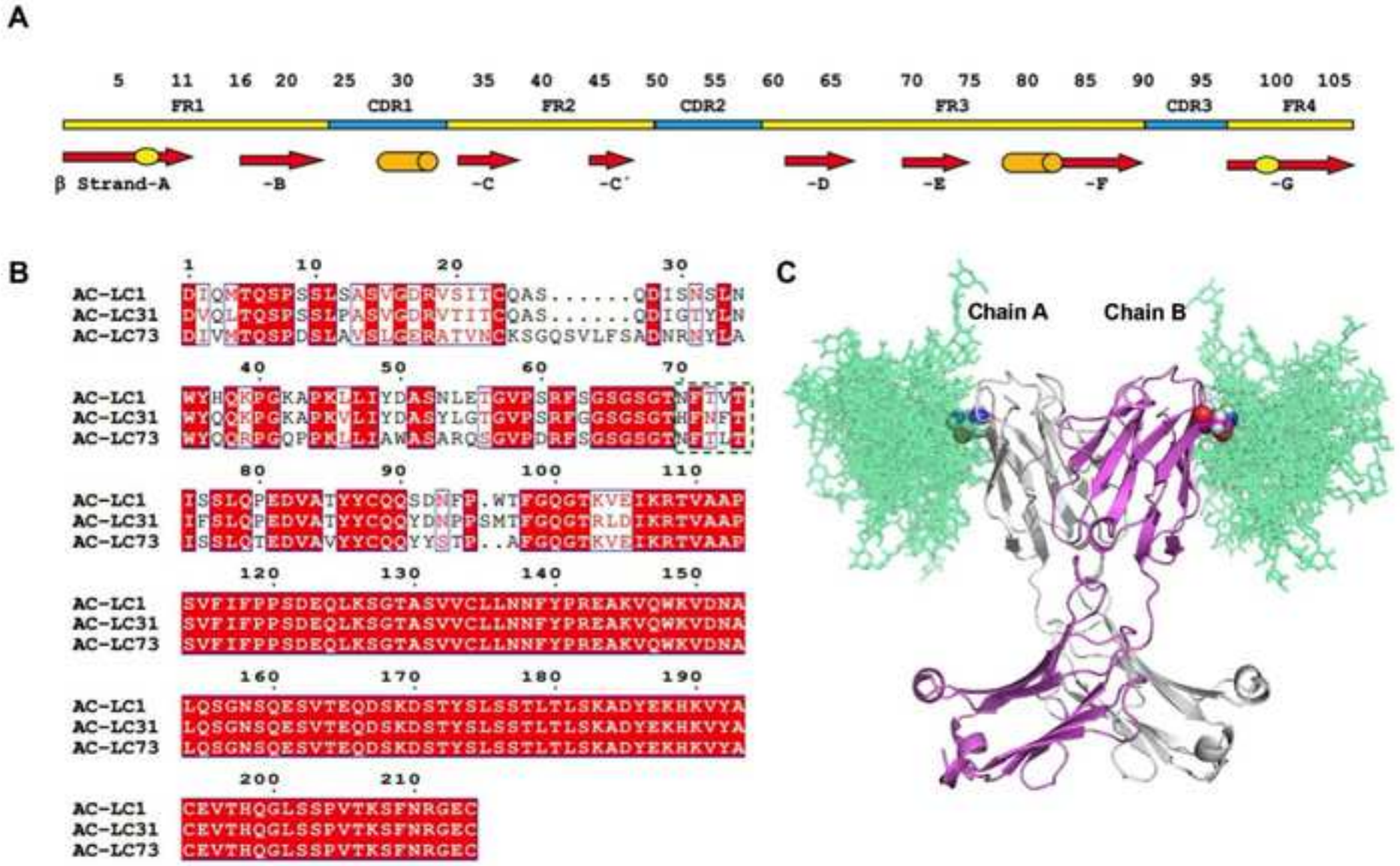

Figure 2

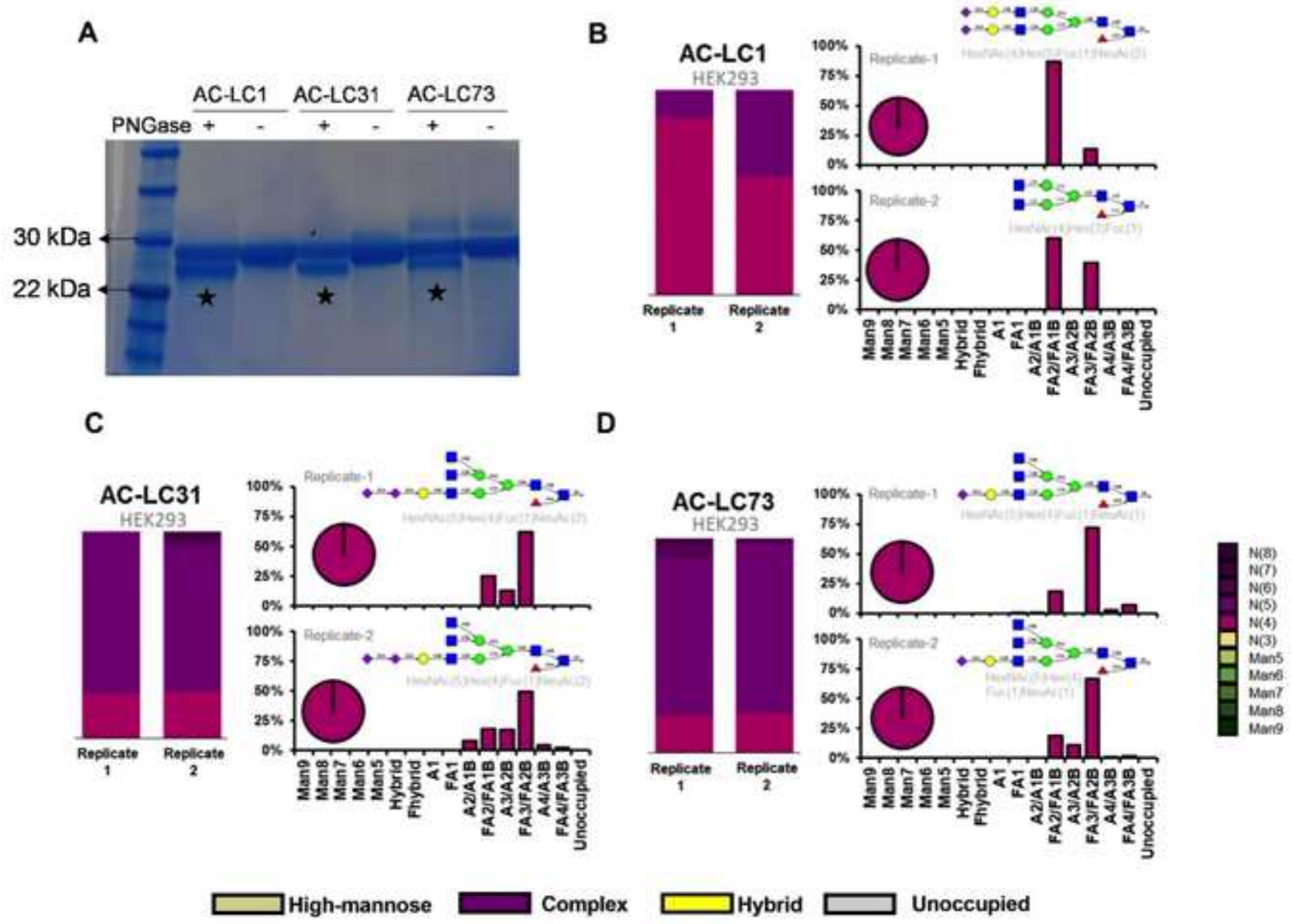

Figure 3

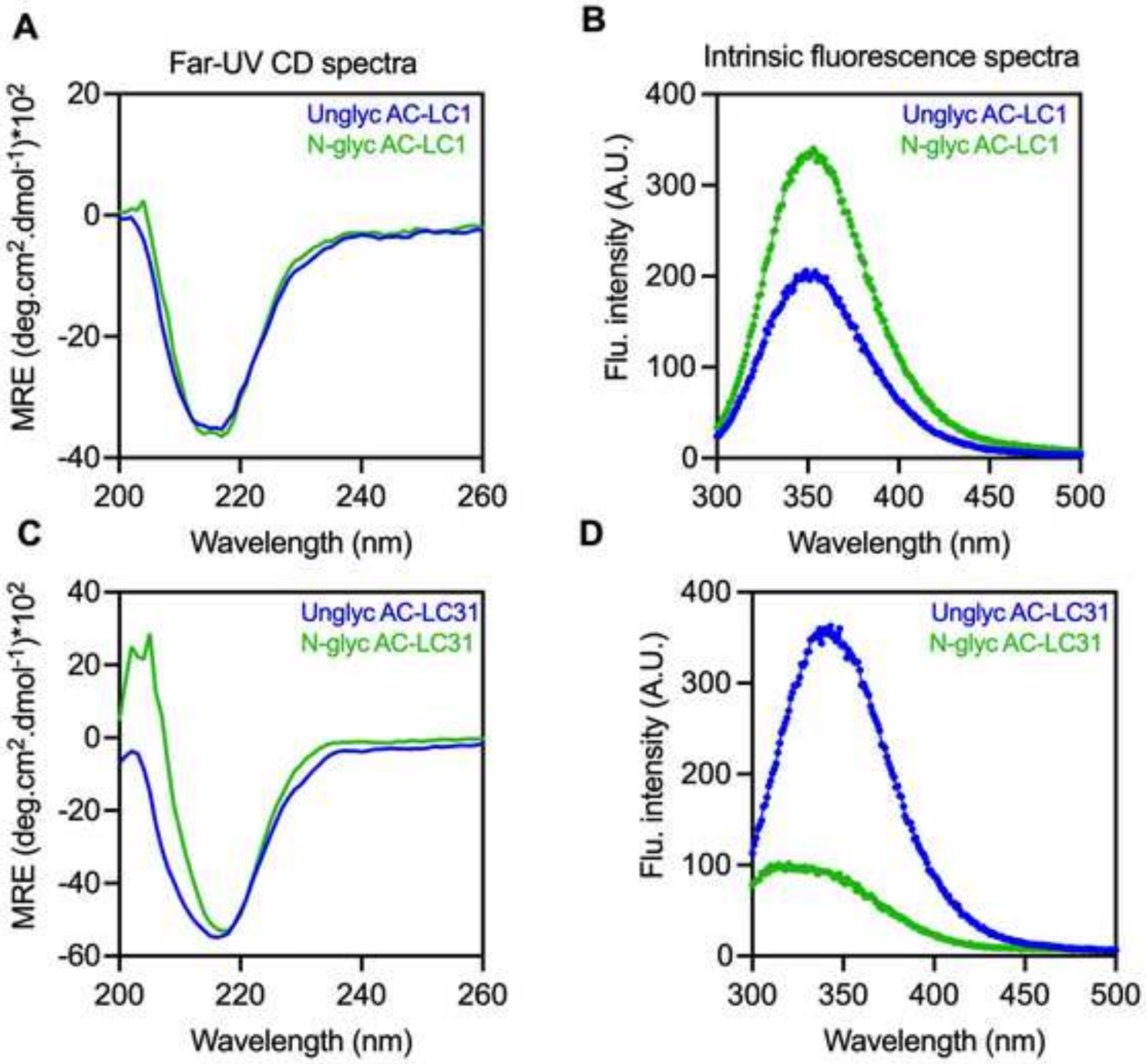

Figure 4

Click here to access/download;Figure;Figure 4_Structure.jpg

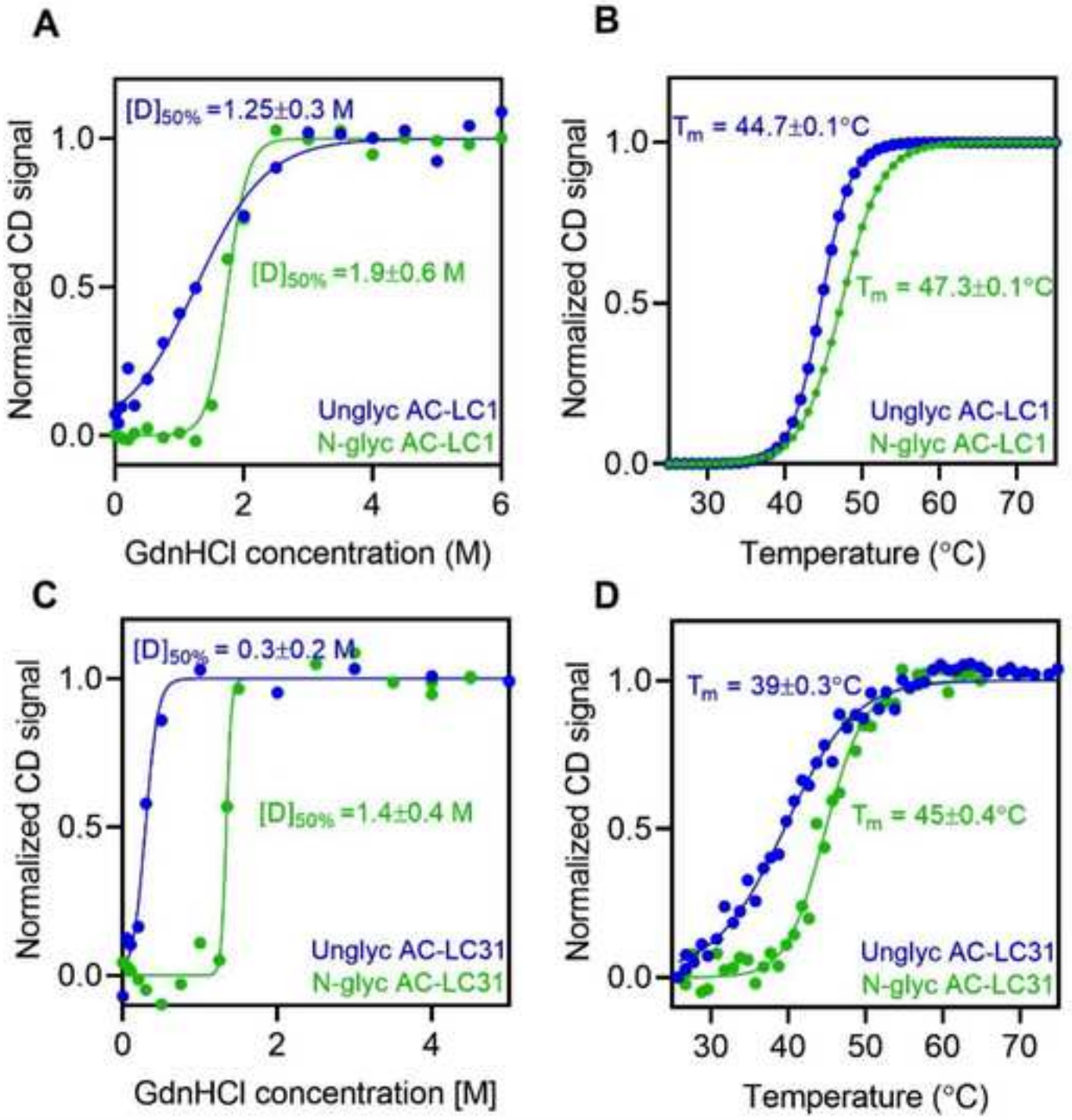

Figure 5

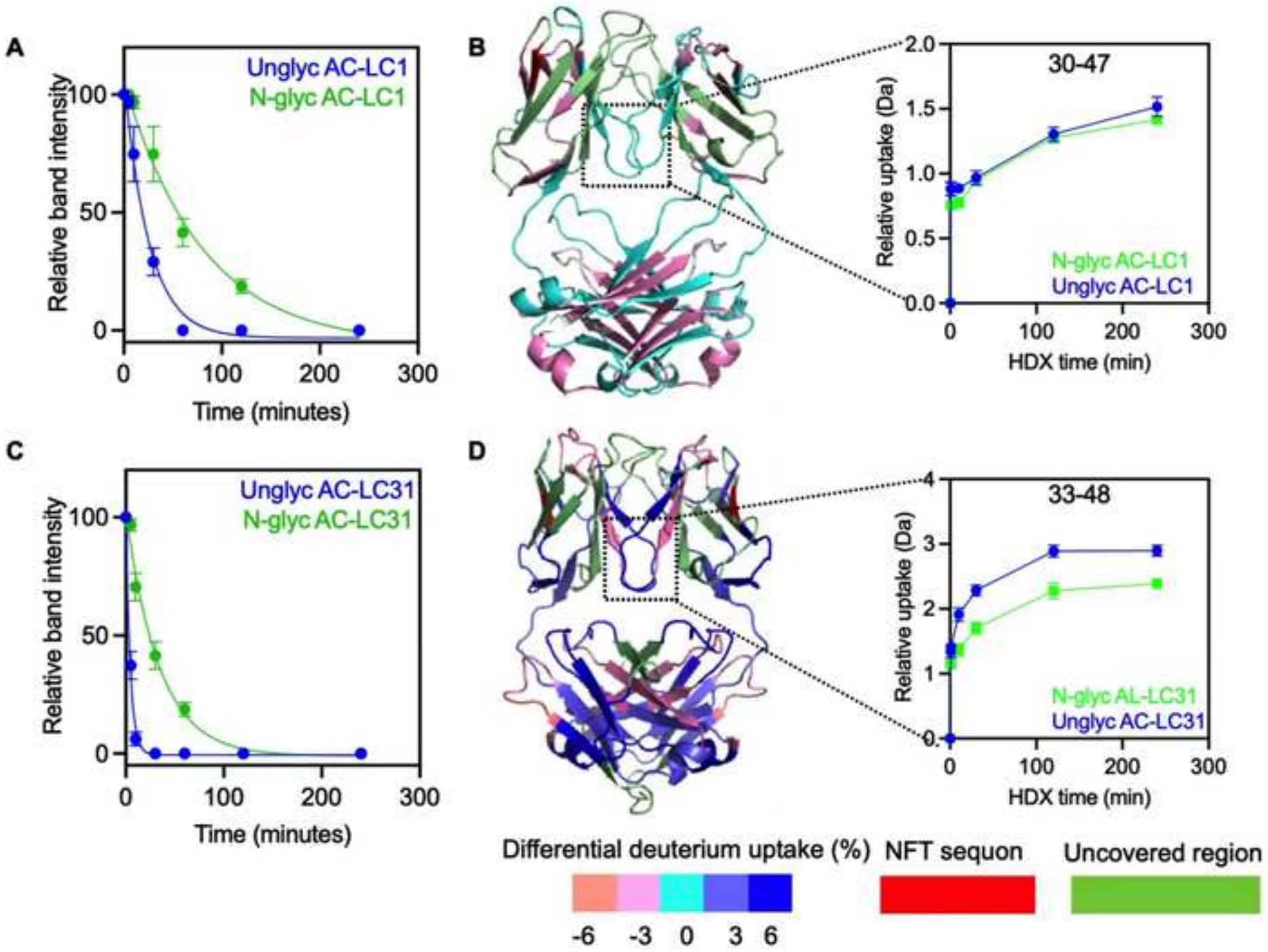

Figure 6

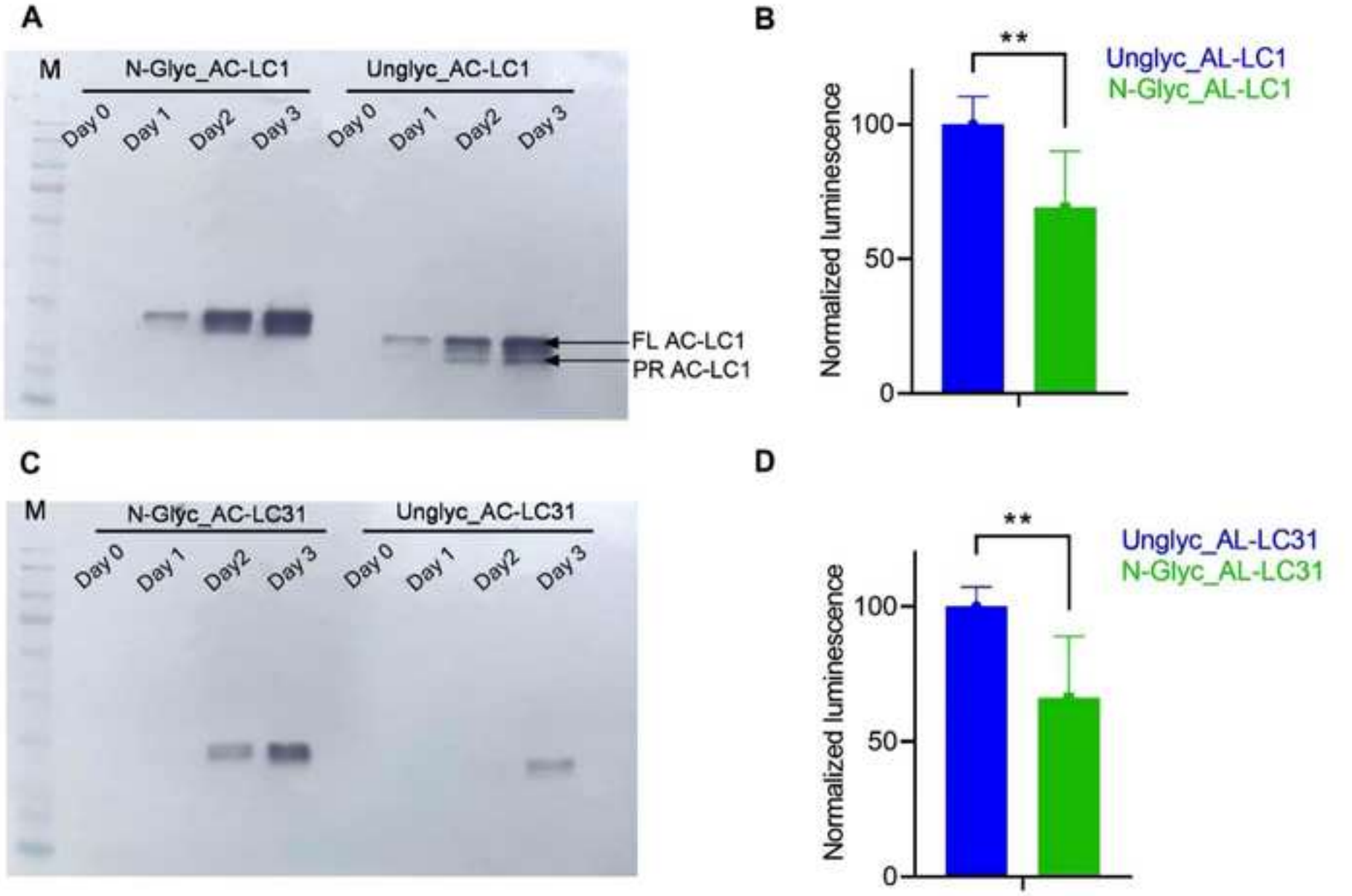

Supporting information

Multifaceted effects of N-glycosylation on amyloidogenic κ light chains in AL amyloidosis

Sarita Puri[1,2&], Valentina Speranzini[1], Monica Russo[3,4], Alice Nevone[3,4], Uriel Petralia[1], Manoj K. Sriramoju[5], Yong-Sheng Wang[5,6], Luca Broggini[1], Giovanni Palladini[3,4], Giampaolo Merlini[3,4], Mario Nuvolone[3,4], Shang-Te Danny Hsu[5,6,7], Stefano Ricagno[1,8&]

1. Department of Biosciences, University of Milan, Italy.
2. Biology Department, Indian Institute of Science Education and Research, Pune, India.
3. Department of Molecular Medicine, University of Pavia, Pavia, Italy.
4. Amyloidosis Research and Treatment Center, Fondazione IRCCS Policlinico San Matteo, Pavia, Italy.
5. Institute of Biological Chemistry, Academia Sinica, Taipei 11529, Taiwan.
6. Institute of Biochemical Sciences, National Taiwan University, Taipei 10617, Taiwan
7. International Institute for Sustainability with Knotted Chiral Meta Matter (WPI-SKCM²), Hiroshima University, 1-3-1 Kagamiyama, Higashi-Hiroshima, Hiroshima 739-8526, Japan.
8. Lead contact

& Corresponding to: Stefano.ricagno@unimi.it & saritapuri@iiserpune.ac.in

Table S1. Thermodynamic stability parameters obtained from chemical unfolding experiment, related to Figure 4.

Protein	$[D]_{50\%}$ (M)	m-value (kcal/ mol/M)	$\Delta G_{NU}^{H_2O}$ (kcal/mol)
Unglyc AC-LC1	1.25±0.3	1.1±0.2	1.37±0.2
N-glyc ACC-LC1	1.90±0.5	6.4±1.5	12.20±1.5
Unglyc AC-LC31	0.3±0.2	7.2±1.5	2.16±0.8
N-glyc ACB-LC31	1.4±0.4	14.7±5.5	20.58±1.2

Table S2. HDX-MS data summary, related to Figure 5.

Datasets	Unglyc AC-LC1 Single peptide	N-glyc AC-LC1 Single peptide	Unglyc AC-LC31	N-glyc AC-LC31	ΔHDX= Unglyc ACLC1 – Nglyc ACLC1	ΔHDX= Unglyc ACLC31 – Nglyc ACLC31
HDX reaction details	5 mM K_2HPO_4, 5 mM KH_2PO_4, in D_2O (pD 7.0), 25°C					
HDX time course (min)	0, 0.5, 1, 10, 30, 120, and 240					
Back exchange	ND					
No. of peptides	70	74	64	49	52	28
Sequence coverage (%)	93.5	92.5	95.4	91.6	76.3	77.8
Average peptide length/ Redundancy	13.8/5.18	13.5/5.44	13.8/4.60	14.0/3.74	11.7/4.04	12.6/2.31
Replicates (technical)	3	3	3	3	3	3

Repeatability (average SD)	0.06 Da	0.09 Da	0.09 Da	0.09 Da	0.1 Da	0.2 Da

Table S3. Peptide-wise significance score of differential uptake by unglycosylated AC-LC1 and N-glycosylated AC-LC1 for the peptide containing residues 29-45 at different exchange times of 0.5 to 240 min, related to Figure 5 .

Predictors	Estimate	SE	t-statistic	p-value	Significance
0.5 min of both states	0.1621	0.1573	1.0305	0.314	NS
1.0 min of both states	0.1463	0.1573	0.9301	0.362	NS
10 min of both states	0.1296	0.1658	0.7817	0.443	NS
30 min of both states	-0.0588	0.1890	-0.3109	0.759	NS
120 min of both states	0.2442	0.1890	1.2917	0.210	NS
240 min of both states	-0.0879	0.1573	-0.559	0.582	NS

1. *NS: Non-significant
2. The estimate here is the observed difference in deuterium uptake (ΔHDX) between unglycosylated LCs and N-glycosylated LCs. Negative value of the estimate means more deuterium uptake by unglycosylated LCs, while a positive difference means more deuterium uptake by N-glycosylated LCs.
3. Standard error (SE): Uncertainty in the estimate. Smaller is the value, the more precise the measurements.
4. The t-statistic shows how big the difference is relative to noise.
5. The p-value shows the significance of the measurements. Small is the value, more significant is the data statistically.

Table S4. Peptide-wise significance score of differential uptake by unglycosylated AC-LC1 and N-glycosylated AC-LC1 for the peptide containing residues 37-46 at different exchange times of 0.5 to 240 min, related to Figure 5.

Predictors	Estimate	SE	t-statistic	p-value	Significance
0.5 min of both states	0.0623	0.1091	0.5712	0.573	NS
1.0 min of both states	0.1955	0.1091	1.7911	0.864	NS
10 min of both states	-0.0191	0.1029	-0.1852	0.855	NS
30 min of both states	0.0103	0.1150	0.0895	0.929	NS
120 min of both states	-0.0715	0.1091	-0.6552	0.519	NS
240 min of both states	-0.1380	0.1029	-1.3415	0.193	NS

Table S5. Peptide-wise significance score of differential uptake by unglycosylated AC-LC1 and N-glycosylated AC-LC1 for the peptide containing residues 119-125 at different exchange times of 0.5 to 240 min, related to Figure 5.

Predictors	Estimate	SE	t-statistic	p-value	Significance
0.5 min of both states	0.0640	0.0674	0.9496	0.351	NS
1.0 min of both states	0.0561	0.0635	0.8831	0.385	NS
10 min of both states	0.1058	0.0635	1.6655	0.108	NS
30 min of both states	0.0260	0.0674	0.3862	0.702	NS
120 min of both states	0.1505	0.0635	2.3695	0.0255	* ⩾95%
240 min of both states	-0.0300	0.0635	-0.4718	0.641	NS

Table S6. Peptide-wise significance score of differential uptake by unglycosylated AC-LC1 and N-glycosylated AC-LC1 for the peptide containing residues 179-195 at different exchange times of 0.5 to 240 min, related to Figure 5.

Predictors	Estimate	SE	t-statistic	p-value	Significance
0.5 min of both states	-0.0304	0.0982	-0.3094	0.759	NS
1.0 min of both states	-0.0022	0.0982	-0.0219	0.983	NS
10 min of both states	-0.0555	0.0982	-0.5658	0.576	NS
30 min of both states	-0.0990	0.0982	-1.0081	0.322	NS
120 min of both states	0.0168	0.0982	0.1713	0.865	NS
240 min of both states	-0.2282	0.0982	-2.3243	0.276	* ⩾95%

Table S7. Peptide-wise significance score of differential uptake by unglycosylated AC-LC31 and N-glycosylated AC-LC31 for the peptide containing residues 5-12 at different exchange times of 0.5 to 240 min, related to Figure 5.

Predictors	Estimate	SE	t-statistic	p-value	Significance
0.5 min of both states	-0.5602	0.1146	-4.888	6.15E-05	***** ⩾99.9%
1.0 min of both states	-0.6453	0.1080	-5.9733	4.33E-06	***** ⩾99.9%
10 min of both states	-0.7992	0.1080	-7.3977	1.60E-07	***** ⩾99.9%
30 min of both states	-0.7633	0.1146	-6.6610	8.53E-07	***** ⩾99.9%
120 min of both states	-0.7676	0.1146	-6.6988	7.82E-07	***** ⩾99.9%
240 min of both states	-0.6840	0.1208	-5.6625	9.16E-06	***** ⩾99.9%

Table S8. Peptide-wise significance score of differential uptake by unglycosylated AC-LC31 and N-glycosylated AC-LC31 for the peptide containing residues 37-48 at different exchange times of 0.5 to 240 min, related to Figure 5.

Predictors	Estimate	SE	t-statistic	p-value	Significance
0.5 min of both states	-0.1807	0.0768	-2.3534	2.61E-02	* ⩾95%
1.0 min of both states	-0.2416	0.0768	-3.1465	4.00E-03	***** ⩾99.9%
10 min of both states	-0.5313	0.0768	-6.9187	1.96E-07	***** ⩾99.9%
30 min of both states	-0.5008	0.0814	-6.1491	1.43E-06	***** ⩾99.9%
120 min of both states	-0.06244	0.0768	-8.1318	9.81E-09	***** ⩾99.9%
240 min of both states	-0.4950	0.0768	-6.4468	6.58E-07	***** ⩾99.9%

Table S9. Peptide-wise significance score of differential uptake by unglycosylated AC-LC31 and N-glycosylated AC-LC31 for the peptide containing residues 107-118 at different exchange times of 0.5 to 240 min, related to Figure 5.

Predictors	Estimate	SE	t-statistic	p-value	Significance
0.5 min of both states	-0.1246	0.1458	-0.8547	4.00E-01	NS
1.0 min of both states	-0.1862	0.1458	-1.2775	2.12E-01	NS
10 min of both states	-0.3067	0.1458	-2.1039	4.48E-02	* ⩾95%
30 min of both states	-0.4385	0.1458	-2.8359	8.56E-03	***** ⩾99.9%
120 min of both states	-0.4460	0.1458	-3.0595	4.96E-03	***** ⩾99.9%
240 min of both states	-0.2406	0.1458	-1.6506	1.10E-01	NS

Table S10. Peptide-wise significance score of differential uptake by unglycosylated AC-LC31 and N-glycosylated AC-LC31 for the peptide containing residues 164-177 at different exchange times of 0.5 to 240 min, related to Figure 5.

Predictors	Estimate	SE	t-statistic	p-value	Significance
0.5 min of both states	-0.2833	0.1053	-2.6894	1.21E-02	** ⩾98.0%
1.0 min of both states	-0.3637	0.1053	-3.4525	1.85E-03	***** ⩾99.9%
10 min of both states	-0.3017	0.1053	-2.8644	7.99E-03	***** ⩾99.9%
30 min of both states	-0.1908	0.1117	-1.7080	9.91E-02	* ⩾95.0%
120 min of both states	-0.2875	0.1053	-2.7295	1.10E-02	** ⩾98.0%
240 min of both states	-0.0549	0.1053	-0.5214	6.06E-01	NS

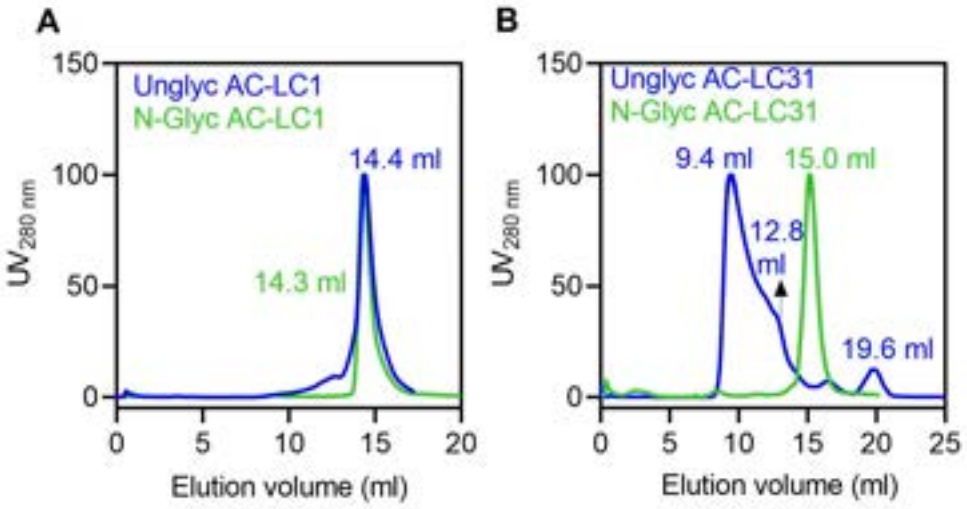

Figure S1. Size-exclusion chromatography (SEC) profiles of purified AC-LC1 and AC-LC31, related to STAR Methods. (A) SEC profiles of unglycosylated AC-LC1 (blue) and N-glycosylated AC-LC1 (green) with an elution volume of 14.4 and 14.3 ml, respectively. (B) SEC profiles of unglycosylated (blue) and N-glycosylated AC-LC31 (green). Unglycosylated AC-LC31 exists in multiple oligomeric forms, which include two broad peaks containing oligomeric forms and a minor contribution from a small size peak, probably a monomeric protein, while glycosylated AC-LC31 shows a single peak at 15.0 ml.

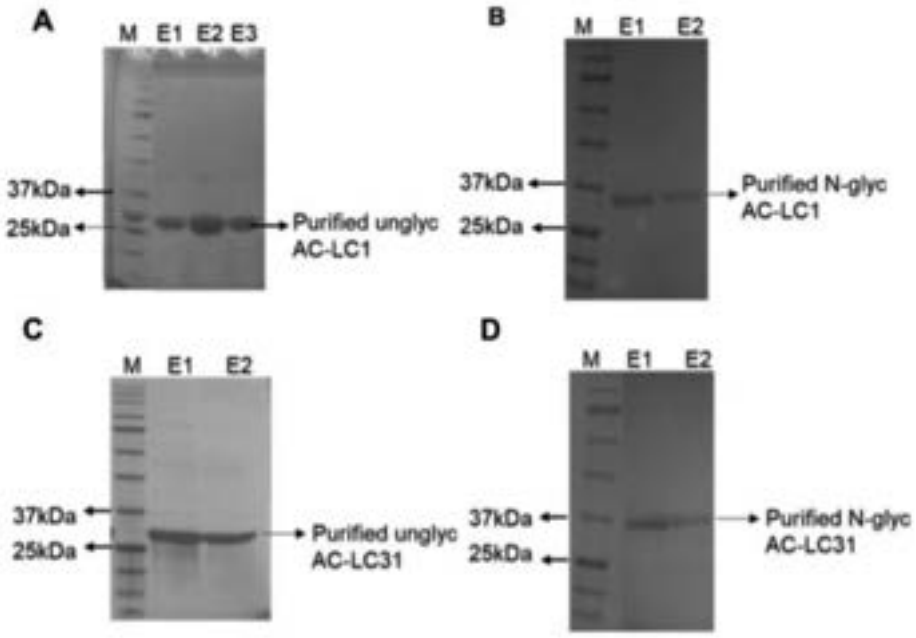

Figure S2. SDS-PAGE gel showing purity levels of AC-LC1 and AL-LC31, related to STAR Methods. (A) SDS-PAGE showing purity levels of unglyc AC-LC1, (B) N-glycosylated AC-LC1, (C) Unglyc AC-LC31, (D) N-glyc AC-LC31.

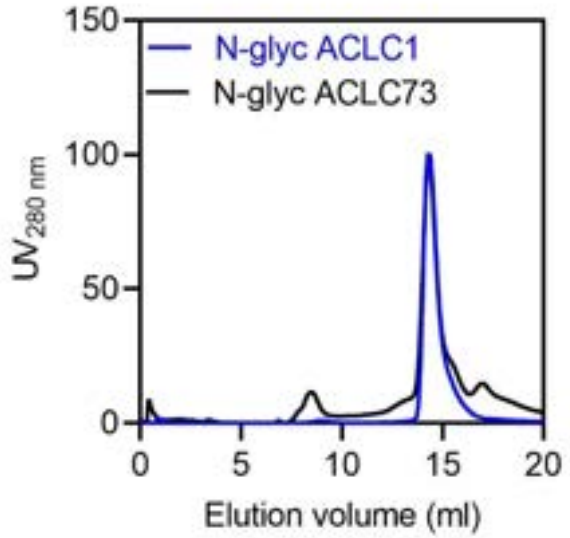

Figure S3. Comparison of size-exclusion chromatography (SEC) profiles of N-glyc AC-LC1 and N-glyc AC-LC73, related to STAR Methods. SEC profiles of N-glycosylated AC-LC1 (blue) and AC-LC73 (black). The major peak at 14.4 ml elution volume shows that N-glycosylated AC-LC73 eluted as a dimer similar to AC-LC1 and AC-LC31.

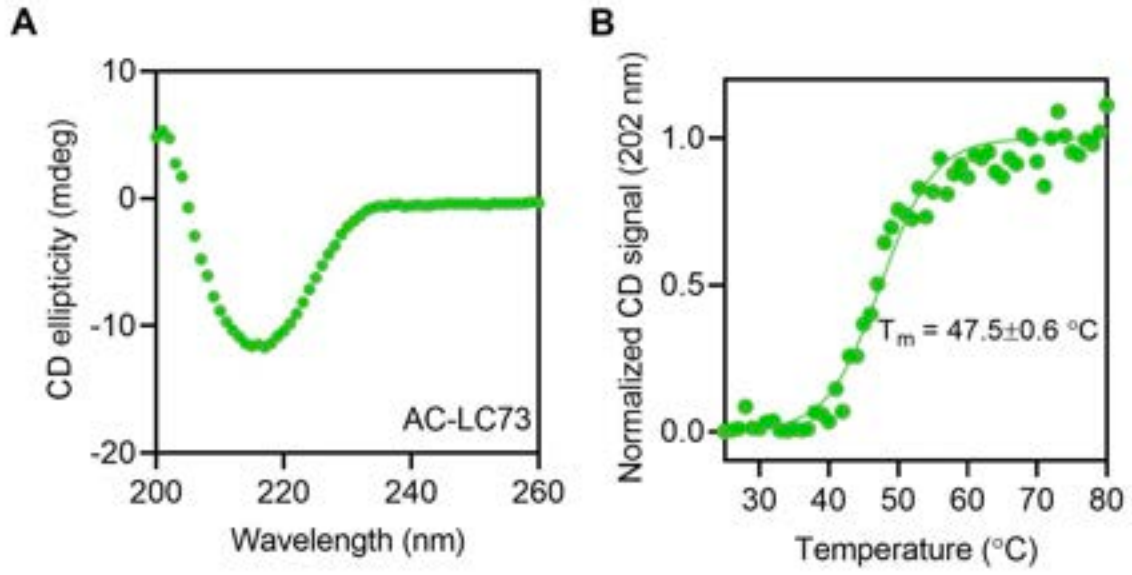

Figure S4. Structure and stability of N-glyc AC-LC73, related to STAR methods. (A) Far-UV CD spectrum of N-glycosylated AC-LC73, which possesses a typical immunoglobulin fold. (B) Thermal unfolding profile of N-glycosylated AC-LC73, having a melting temperature of 47.5±0.6 °C.

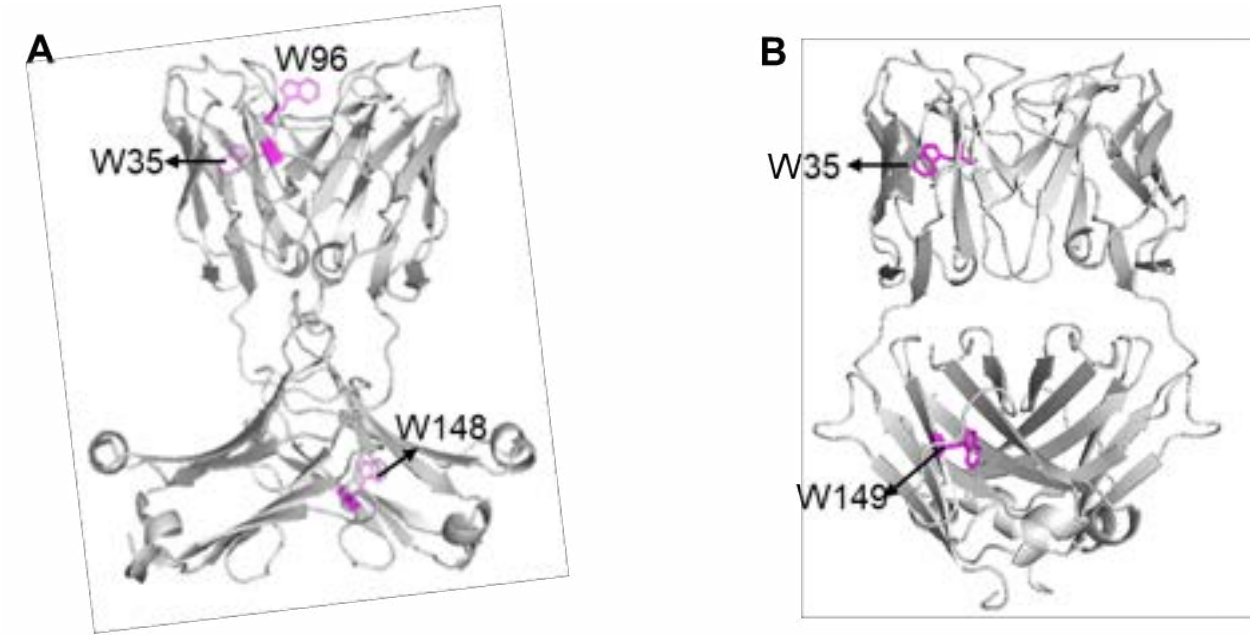

Figure S5. Cartoon showing location of tryptophan (W) residues in AC-LC1 and AC-LC31, related to Figure 3. (A) Tryptophans (W35, W96 and W148,) arrangements on AlphaFold predicted model of AC-LC1. (B) Tryptophans (W35, and W149) arrangements on AlphaFold predicted model of AC-LC31.

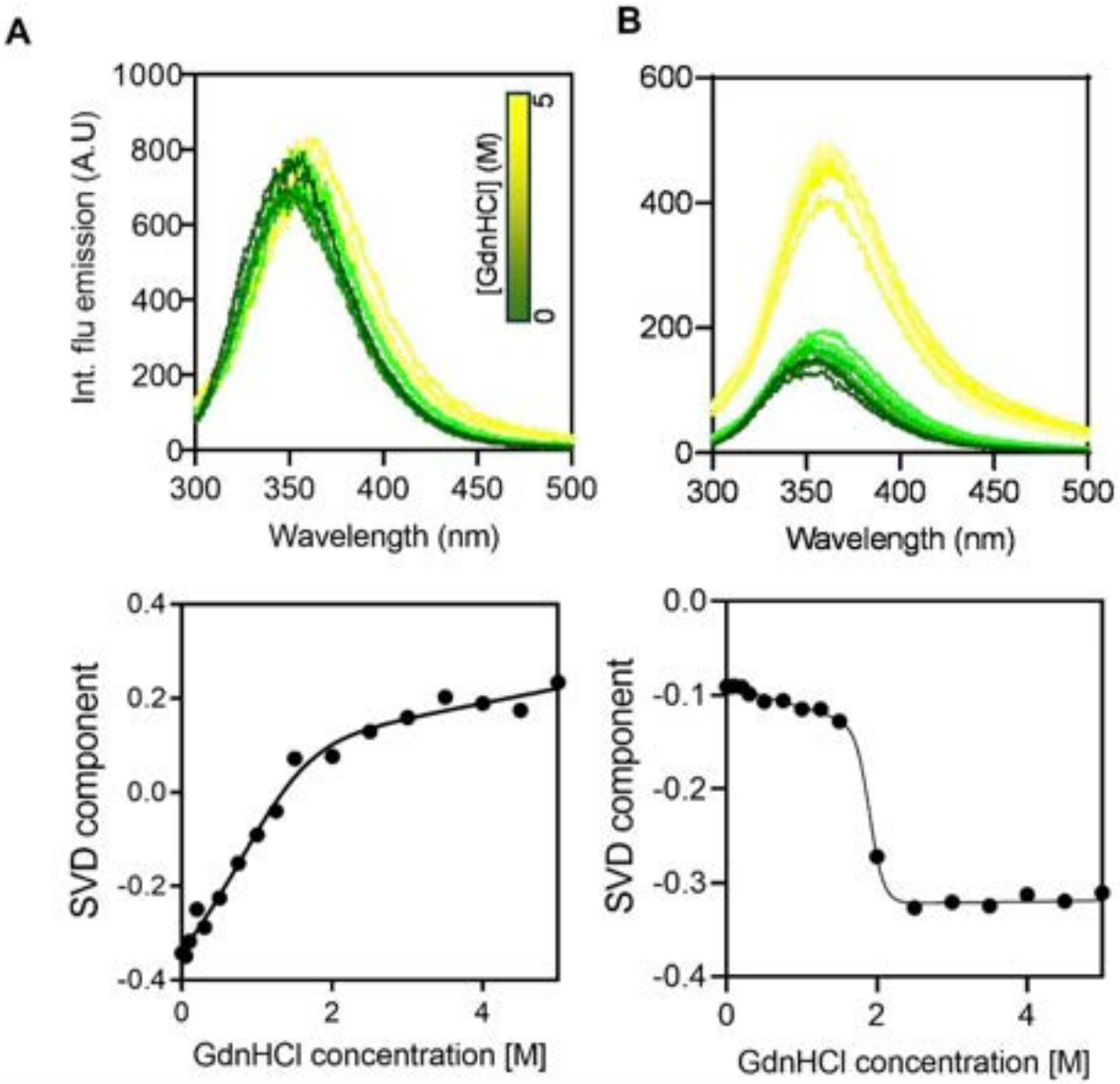

Figure S6. Raw data of chemical unfolding studies of unglycosylated and N-glycosylated AC-LC1, related to Figure 4. (A) The top panel shows intrinsic fluorescence spectra of unglycosylated AC-LC1 at GdnHCl concentrations ranging from 0 to 5 M, with a color gradient from green to yellow. The lower panel is the singular value decomposition (SVD) at different GdnHCl concentrations. (B) The top panel shows intrinsic fluorescence spectra of N-glycosylated AC-LC1 at GdnHCl concentrations ranging from 0 to 5 M, with a color gradient from green to yellow. The lower panel is the singular value decomposition (SVD) at different GdnHCl concentrations.

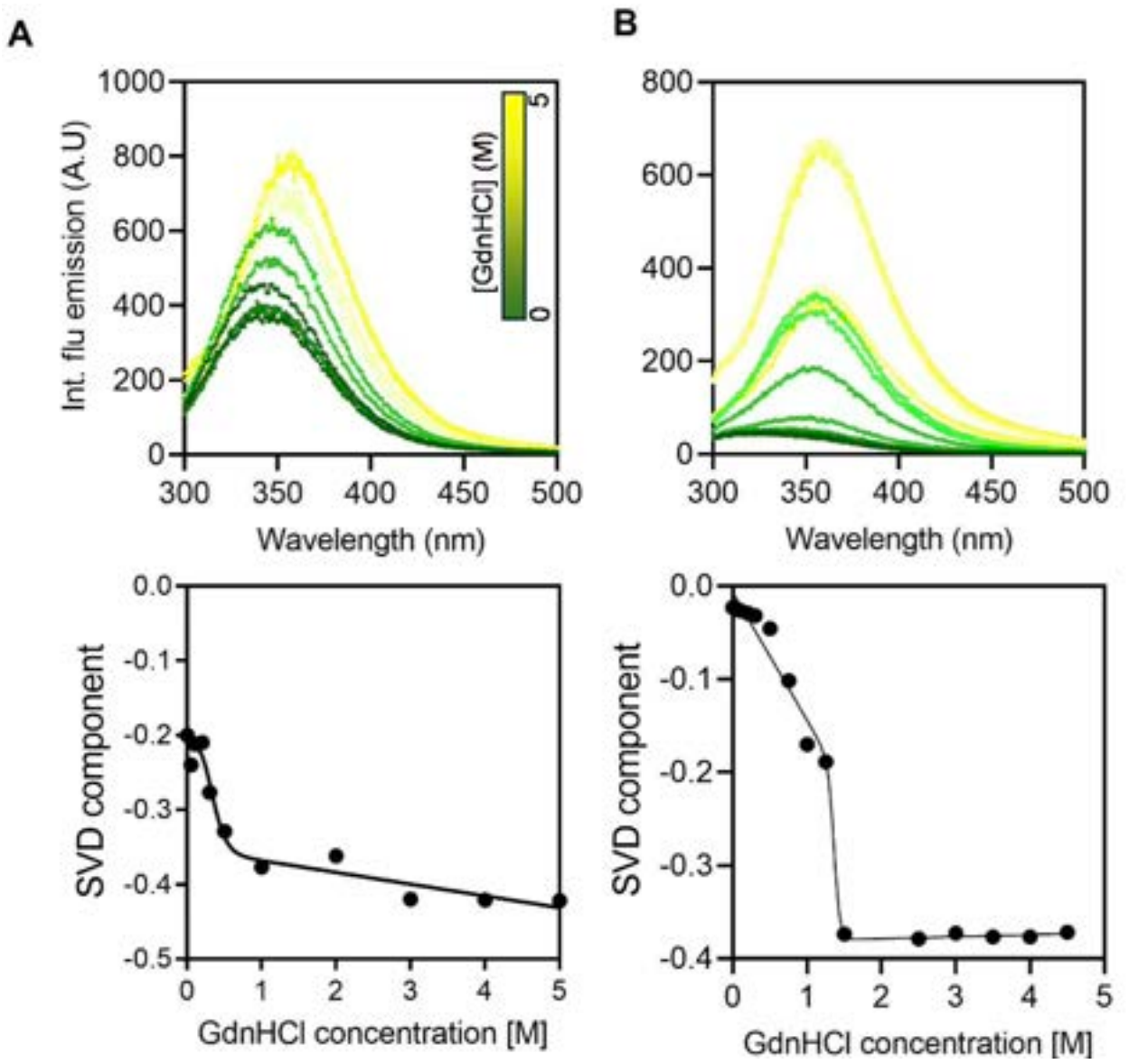

Figure S7. Raw data of chemical unfolding studies of unglycosylated and N-glycosylated AC-LC1, related to Figure 4. (A) The top panel shows intrinsic fluorescence spectra at different GdnHCl concentrations, ranging from 0 to 5 M, in a color gradient of green to yellow for unglycosylated AC-LC31. The lower panel is the singular value decomposition (SVD) at different GdnHCl concentrations. (B) The top panel shows intrinsic fluorescence spectra at different GdnHCl concentrations, ranging from 0 to 5 M, in a color gradient of green to yellow for N-glycosylated AC-LC31. The lower panel is the singular value decomposition (SVD) at different GdnHCl concentrations.

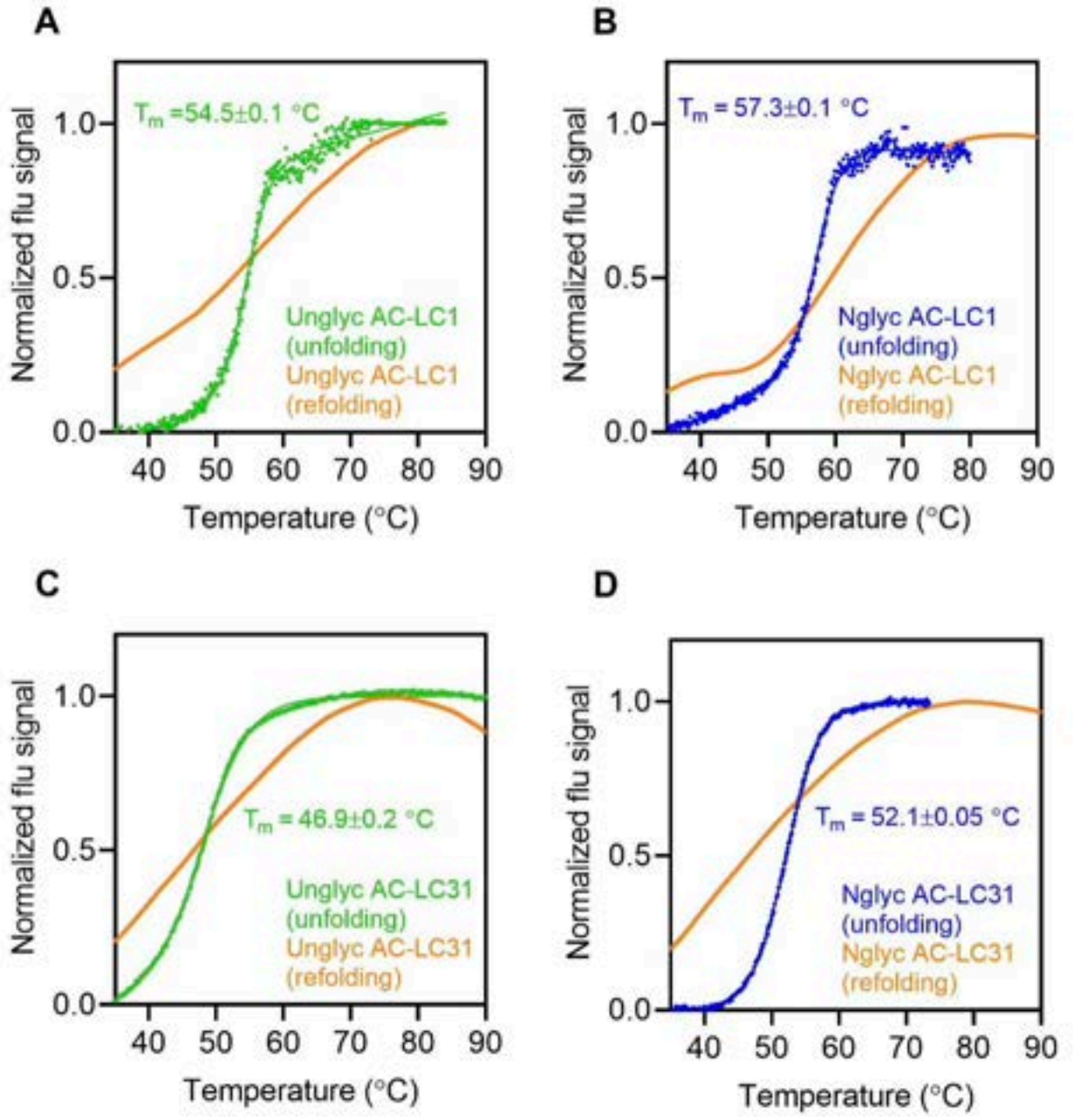

Figure S8. Thermal unfolding and refolding profiles of AC-LC1 and AC-LC31 in their uglycosylared and N-glycosylated forms, related to Figure 4. (A) Thermal unfolding (green) and refolding (orange) profiles of unglycosylated AC-LC1. (B) Thermal unfolding (blue) and refolding (orange) profiles of N-glycosylated AC-LC1. (C) Thermal unfolding (green) and refolding (orange) profiles of unglycosylated AC-LC31. (D) Thermal unfolding (blue) and refolding (orange) profiles of N-glycosylated AC-LC31. Non-overlapping profiles suggest that thermal unfolding of both unglycosylated and N-glycosylated LCs are irreversible.

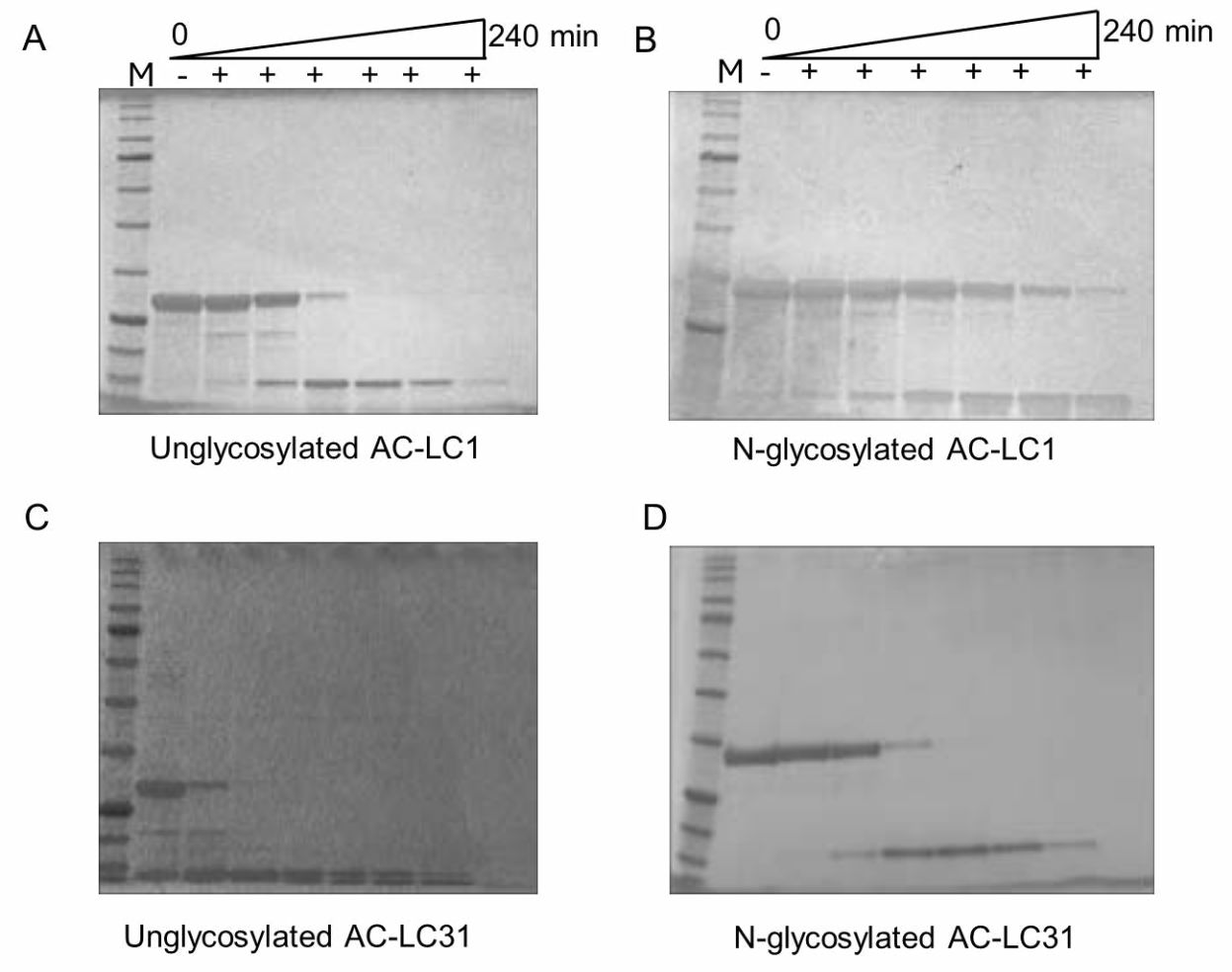

Figure S9. Limited proteolysis assay, related to Figure 5. (A) SDS-PAGE showing limited proteolysis of unglycosylated AC-LC1 with trypsin in a 1:50 (enzyme: protein) ratio at different time points of 0 to 240 min. (B) Glycosylated AC-LC1 with the same enzyme concentration and incubation conditions. (C) Unglycosylated AC-LC31. (D) Glycosylated AC-LC31.

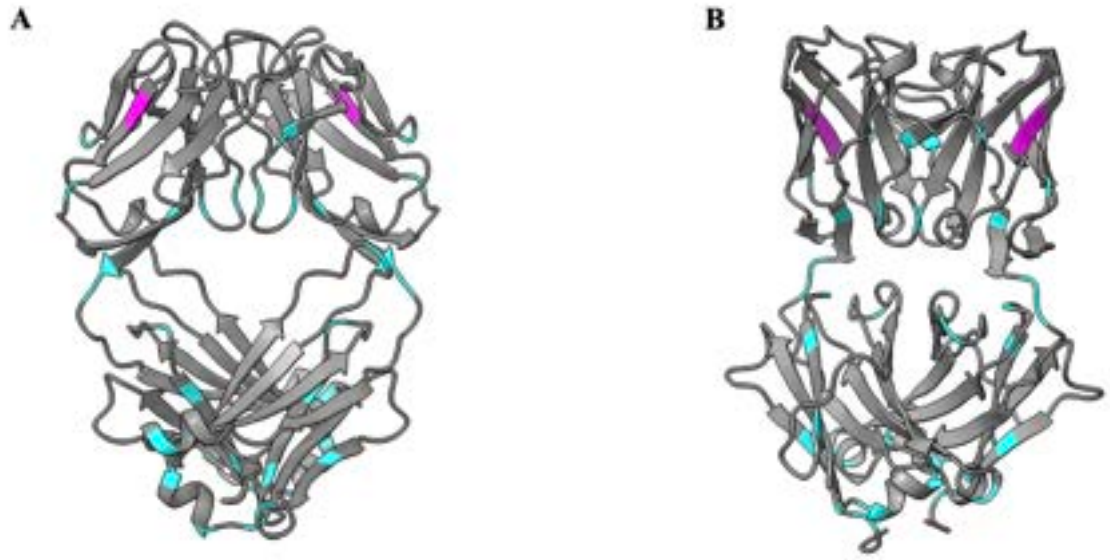

Figure S10. Mapping of potential trypsin digestion sites, related to Figure 5. (A) AC-LC1 model. (B) AC-LC31 model. The NFT sequon is shown in magenta, and potential trypsin digestion sites are in cyan.

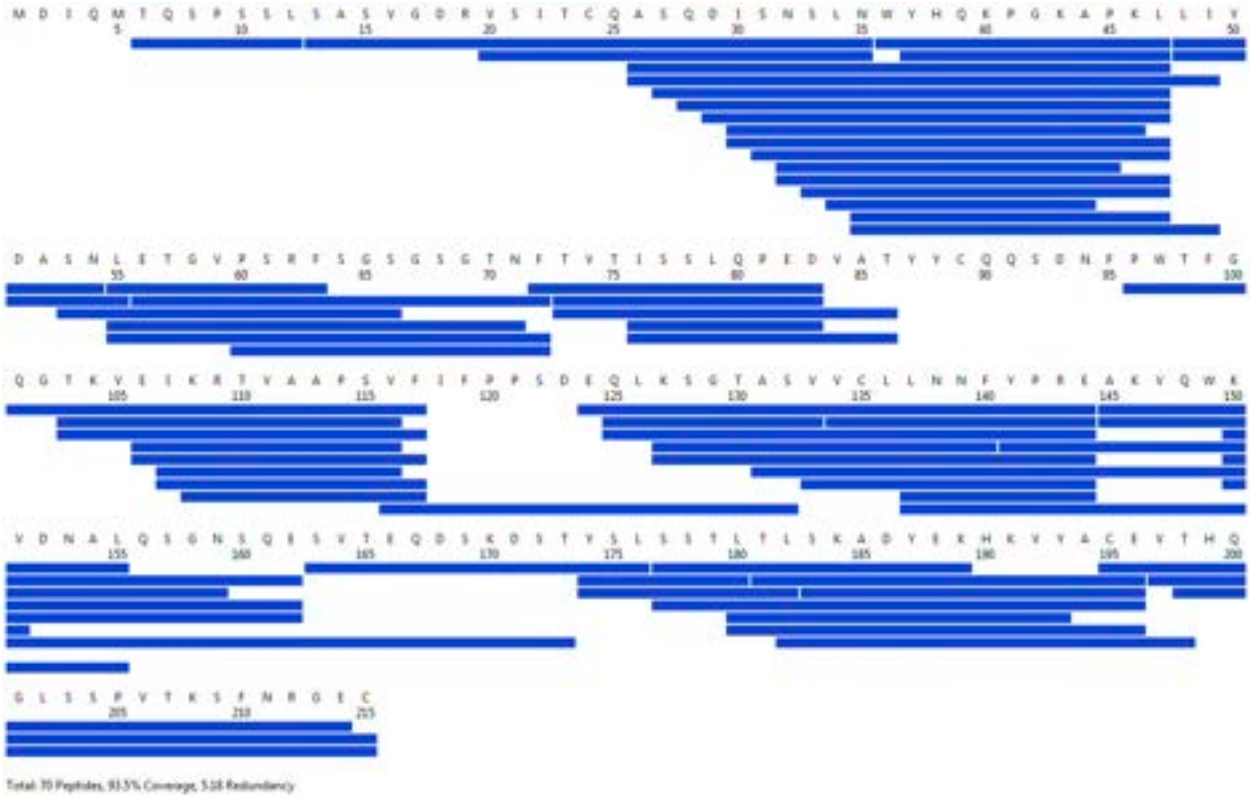

Figure S11. Coverage map, related to Figure 5 and STAR methods. Coverage map obtained after pepsin digestion of unglycosylated AC-LC1. The total number of peptides is 70, coverage is 93.5%, with a redundancy of 5.18. The average of all peptide lengths is 13.8 residues.

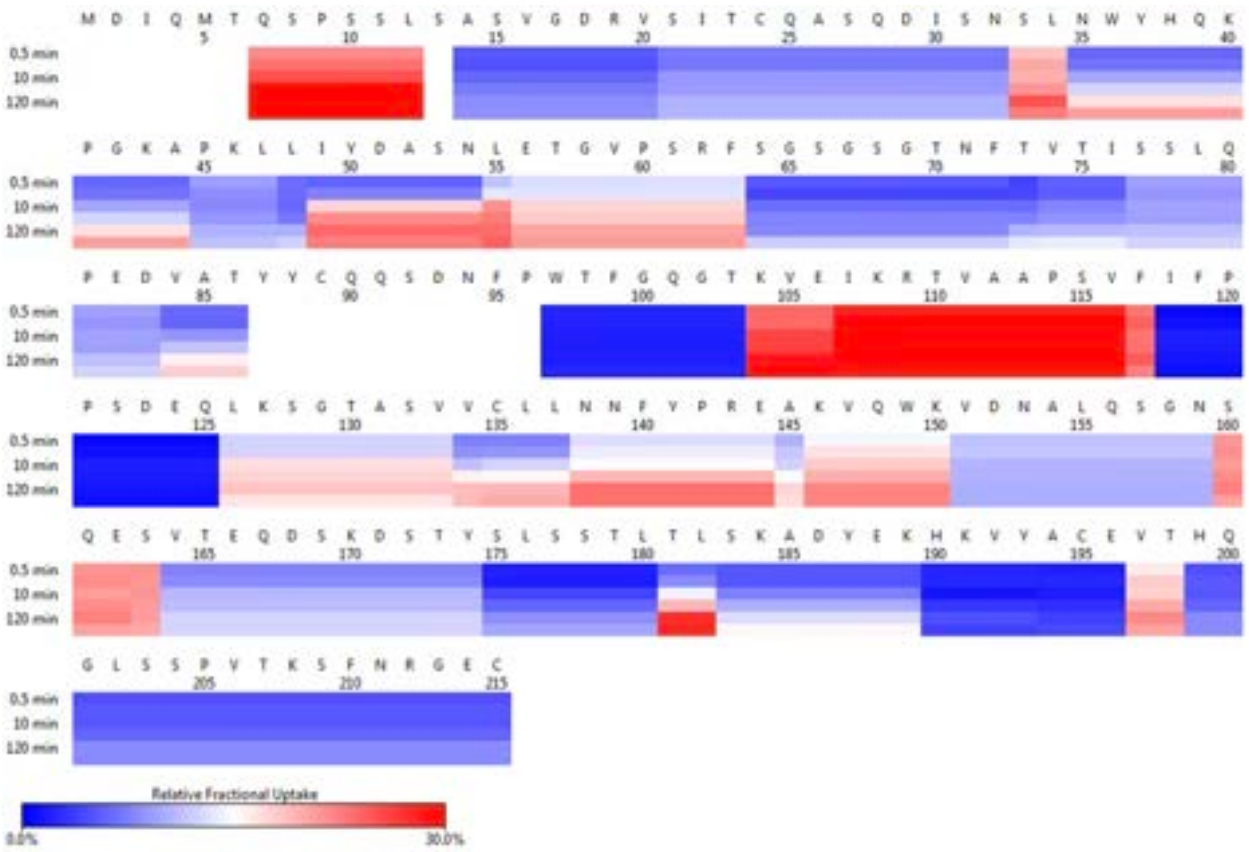

Figure S12. Heat map, related to Figure 5 and STAR methods. Heat map showing deuterium uptake by different peptides of unglycosylated AC-LC1 in a gradient of blue-to-white-to-red for lower to higher uptakes.

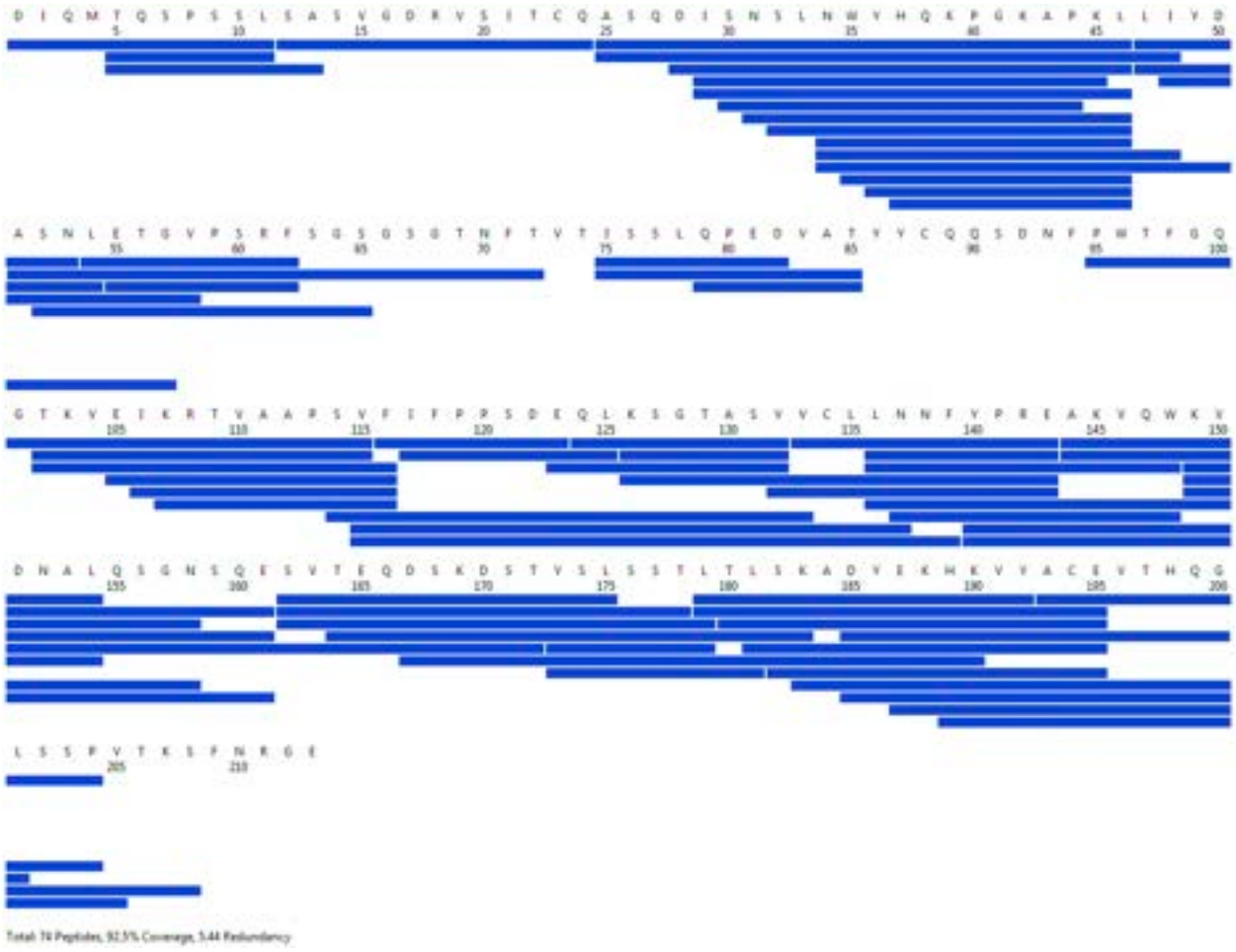

Figure S13. Coverage map, related to Figure 5 and STAR methods. Coverage map obtained after pepsin digestion of glycosylated AC-LC1. The total number of peptides is 74, with 92.5% coverage and a redundancy of 5.44. The average length of all peptides is 13.5.

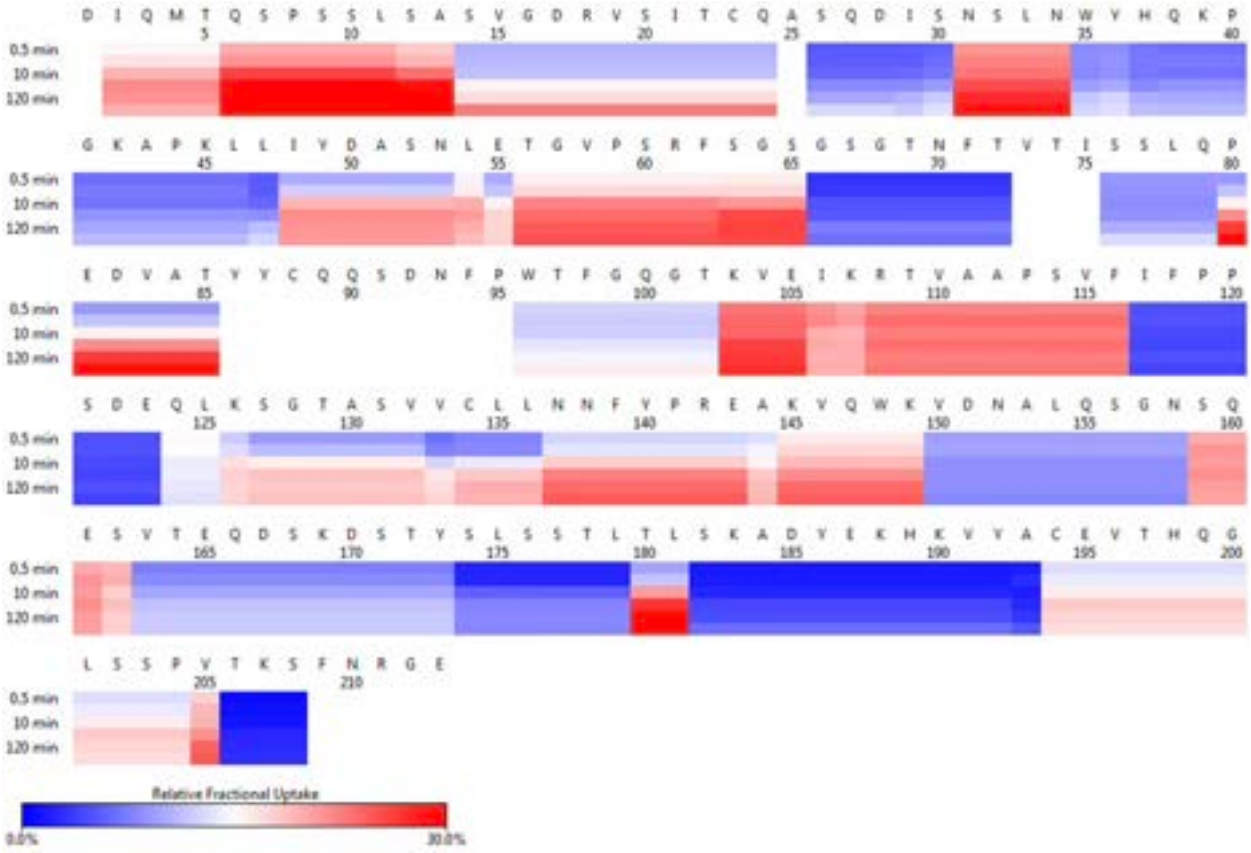

Figure S14. Heat map, related to Figure 5 and STAR methods. Heat map showing deuterium uptake by different peptides of glycosylated AC-LC1 in a gradient of blue-to-white-to-red for less to higher uptakes.

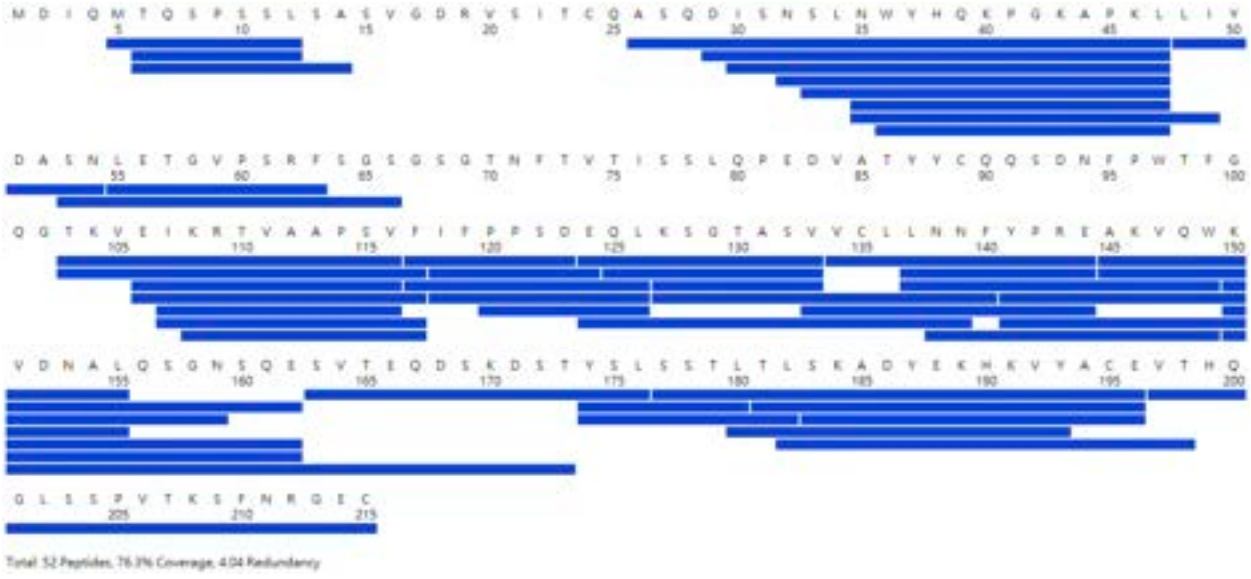

Figure S15. Coverage map, related to Figure 5 and STAR methods. Coverage map of common peptides between unglycosylated and glycosylated AC-LC1. The total number of

peptides is 52, with a coverage of 76.3 and redundancy of 4.04. The average length of all peptides is 13.8.

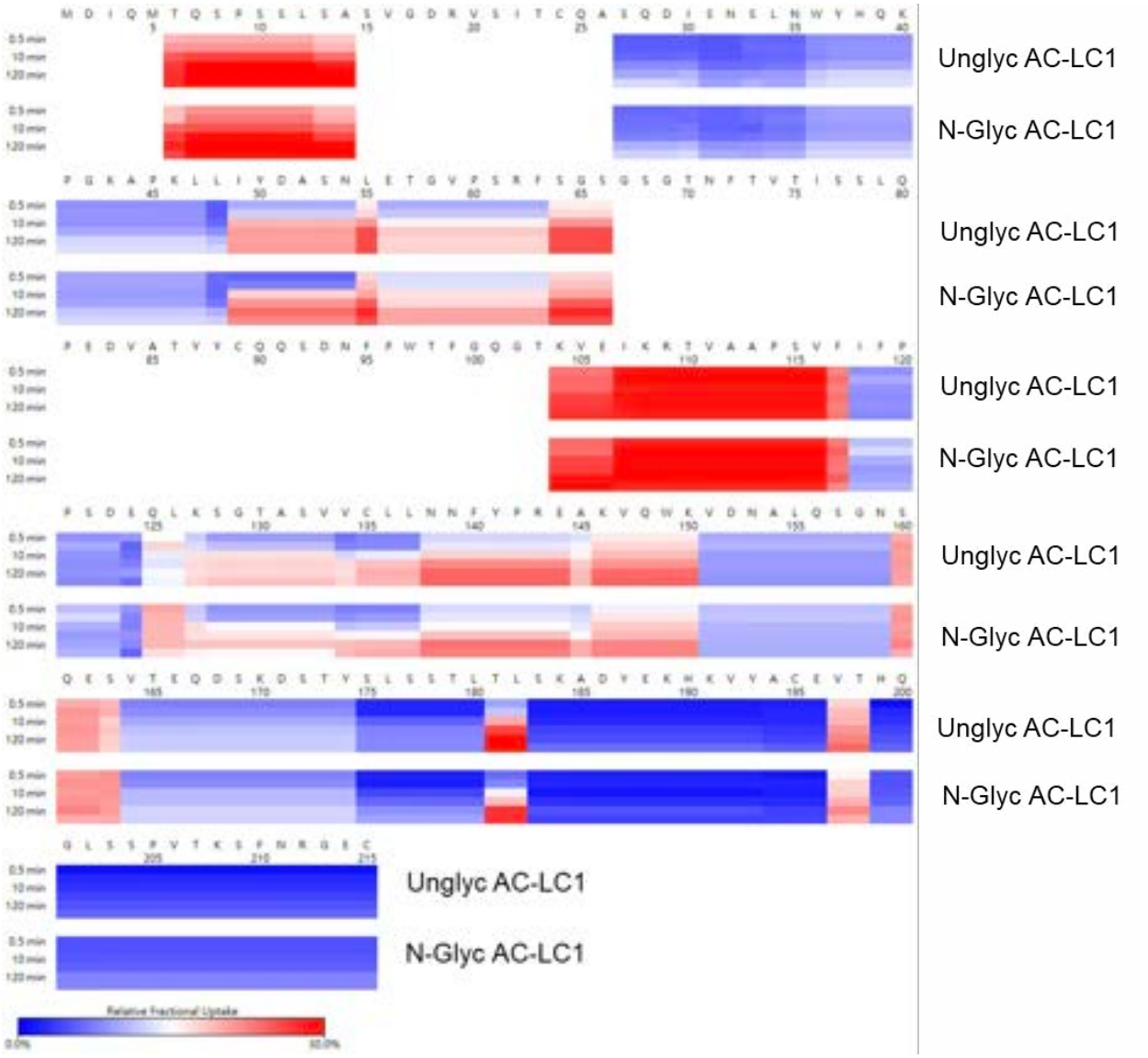

Figure S16. Heat map, related to Figure 5 and STAR methods. Heat map showing deuterium uptake by common peptides between unglycosylated and glycosylated AC-LC1.

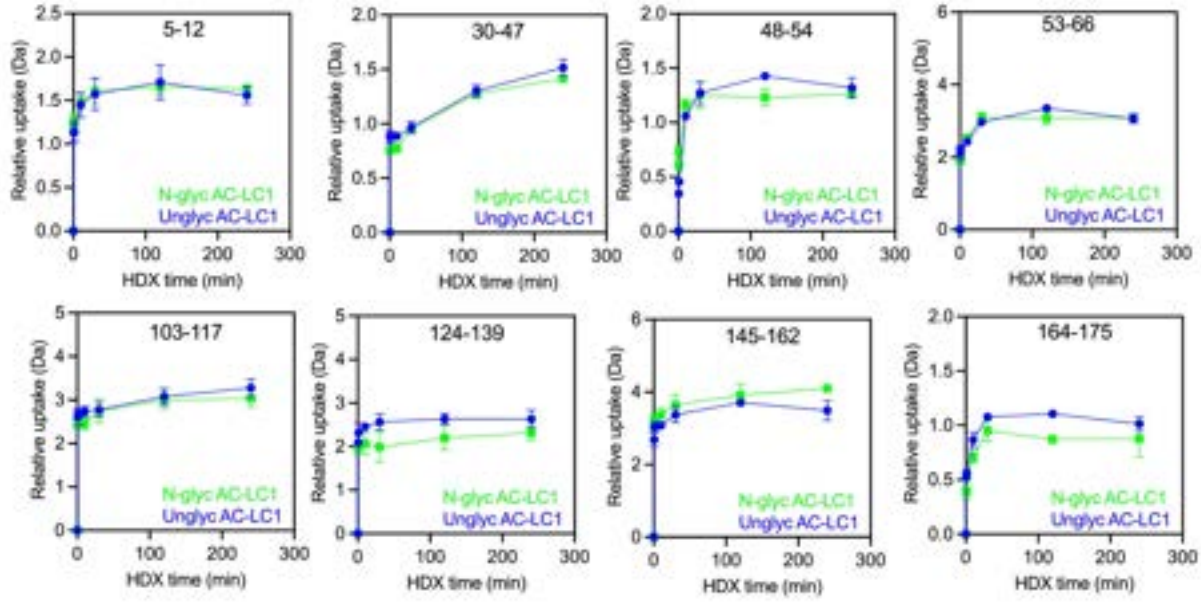

Figure S17. HDX-uptake kinetics plots obtained from Dynmax, related to Figure 5. HDX-uptake kinetics of relative deuterium uptake of the selected common peptides between N-glyc AC-LC1 (green) and unglyc AC-LC1 (blue). The error bars represent the standard deviation with respect to each exchange.

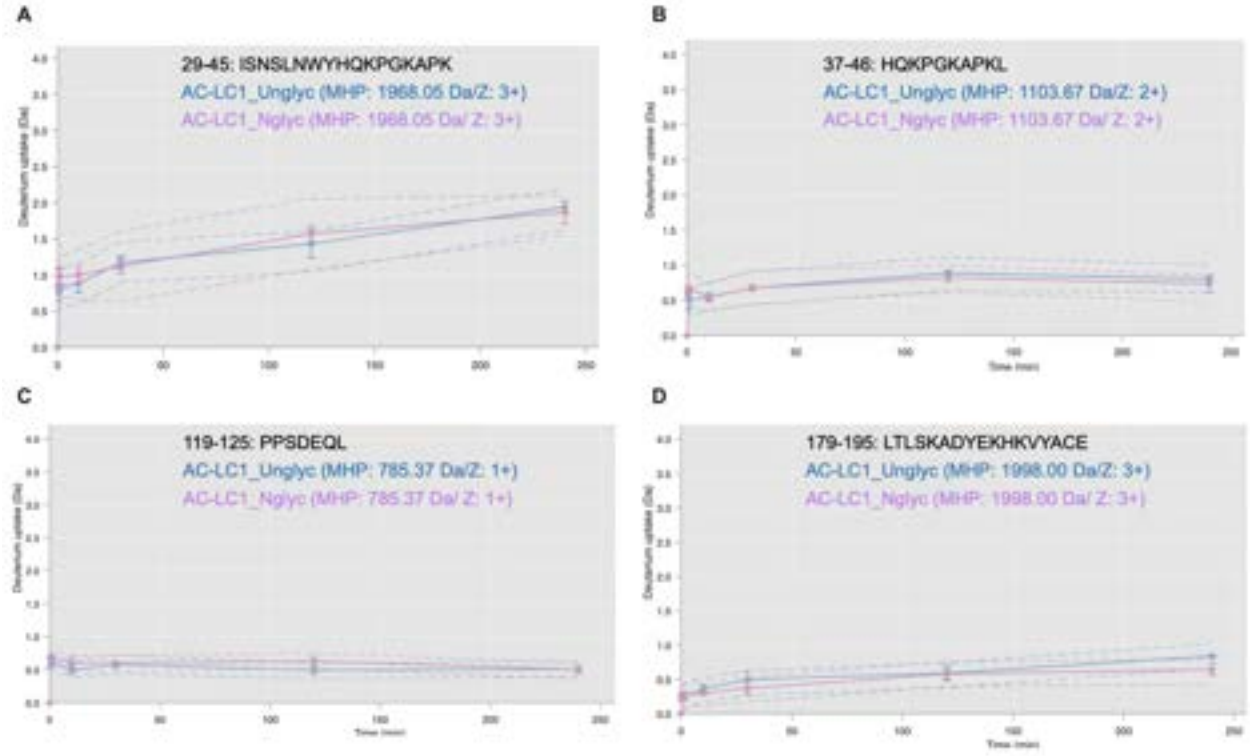

Figure S18. HDX-uptake kinetics plots obtained from Deutero 2, related to Figure 5. HDX-uptake kinetics of relative deuterium uptake of the selected common peptides between N-glyc

AC-LC1 (pink) and unglyc AC-LC1 (blue) by Deuteros 2.0 software. The error bars represent the standard deviation with respect to each exchange.

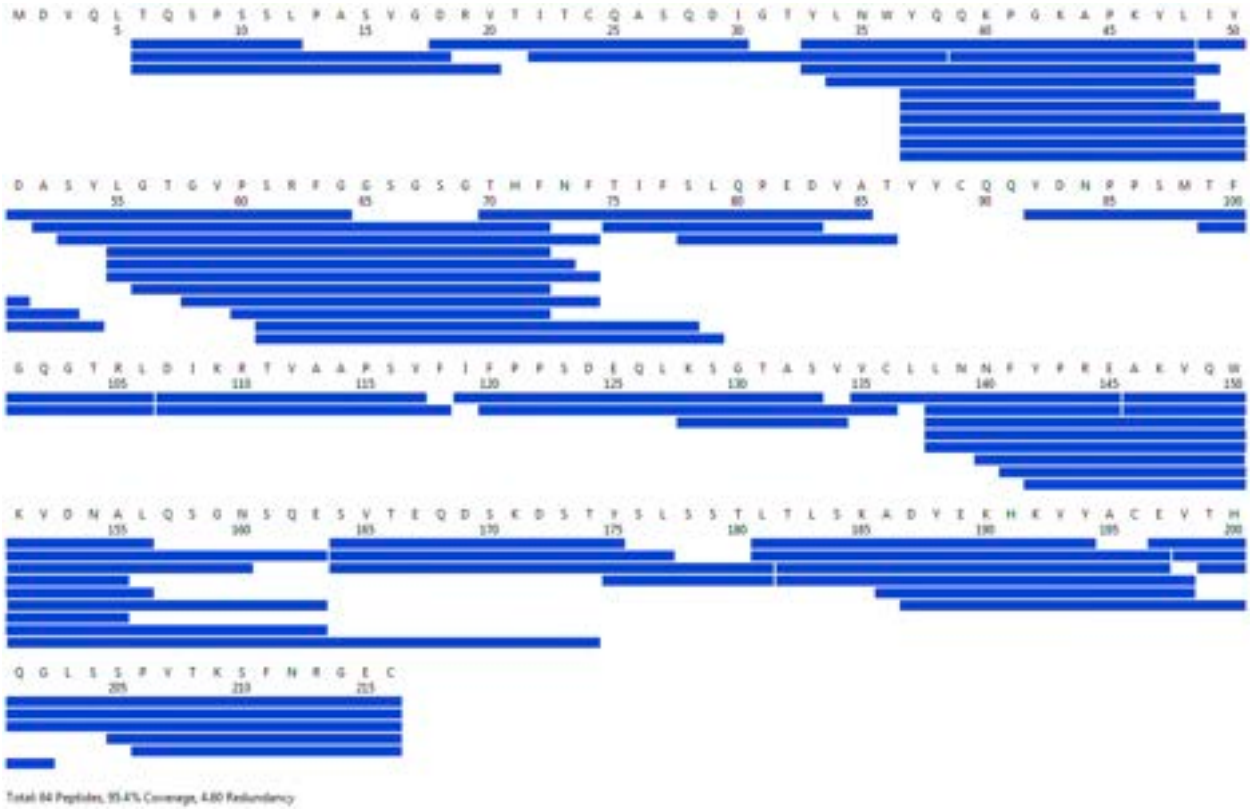

Figure S19. Coverage map, related to Figure 5 and STAR methods. Coverage map on pepsin digestion of unglycosylated AC-LC31. The total number of peptides is 64, coverage is 95.4% with a redundancy of 4.60. The average length of all peptides is 14.0.

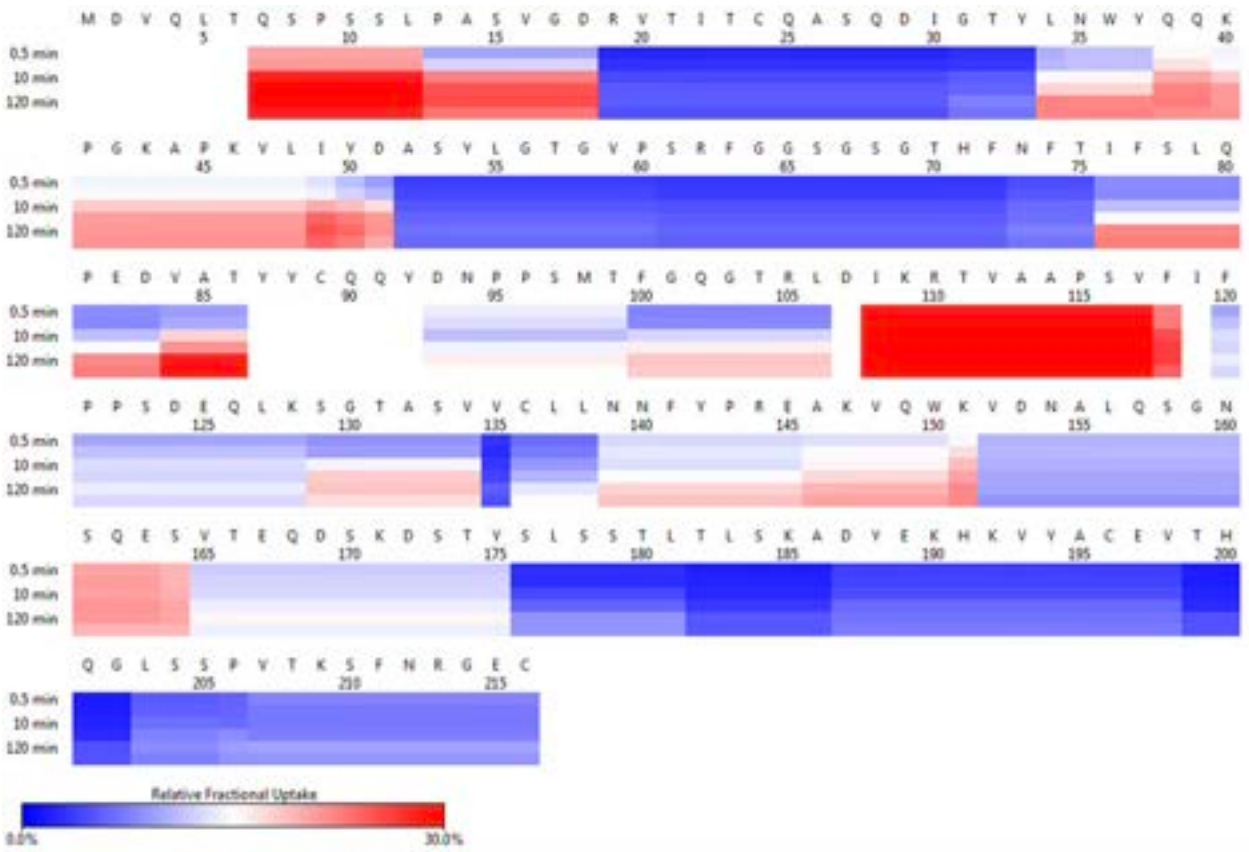

Figure S20. Heat map, related to Figure 5 and STAR methods. Heat map showing deuterium uptake by different peptides of unglycosylated AC-LC31 in a gradient of blue-to-white-to-red for less to higher uptakes.

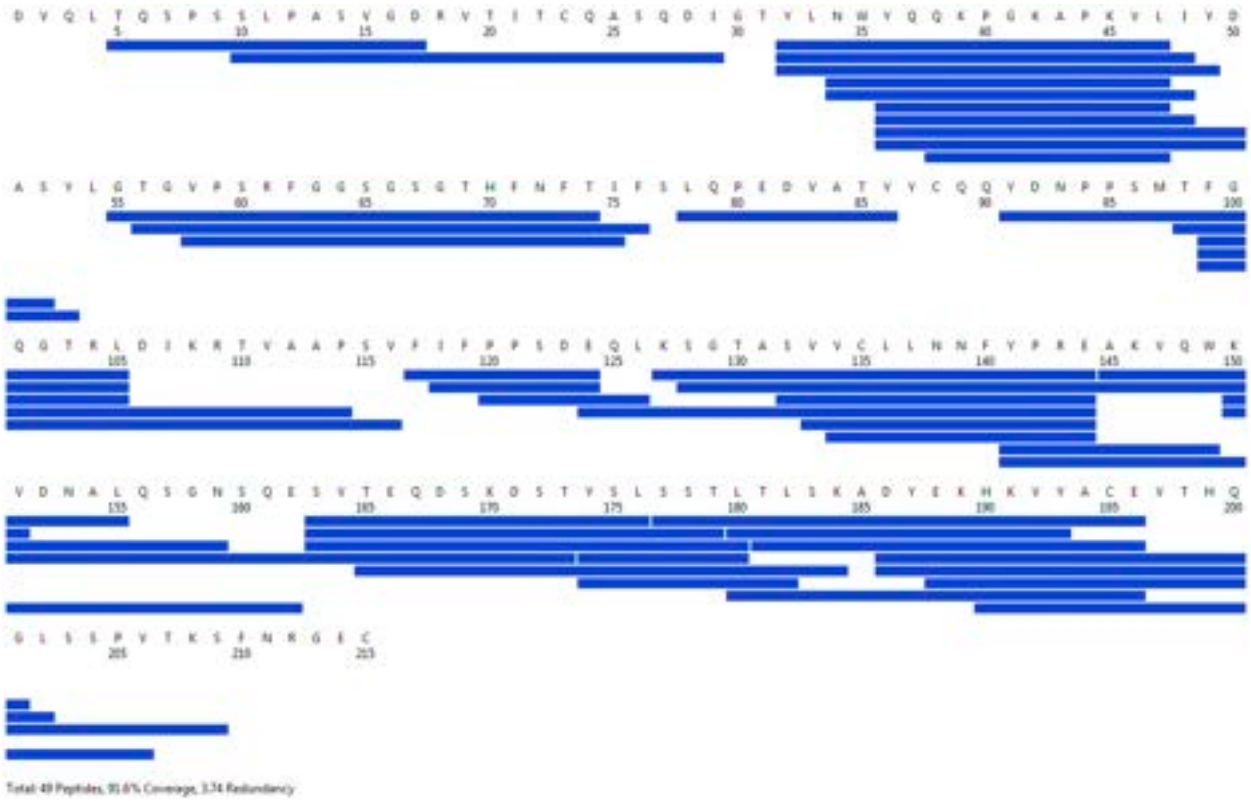

Figure S21. Coverage map, related to Figure 5 and STAR methods. Coverage map on pepsin digestion of glycosylated AC-LC31. The total number of peptides is 49, with 91.6% coverage and a redundancy of 3.74. The average length of all peptides is 11.7

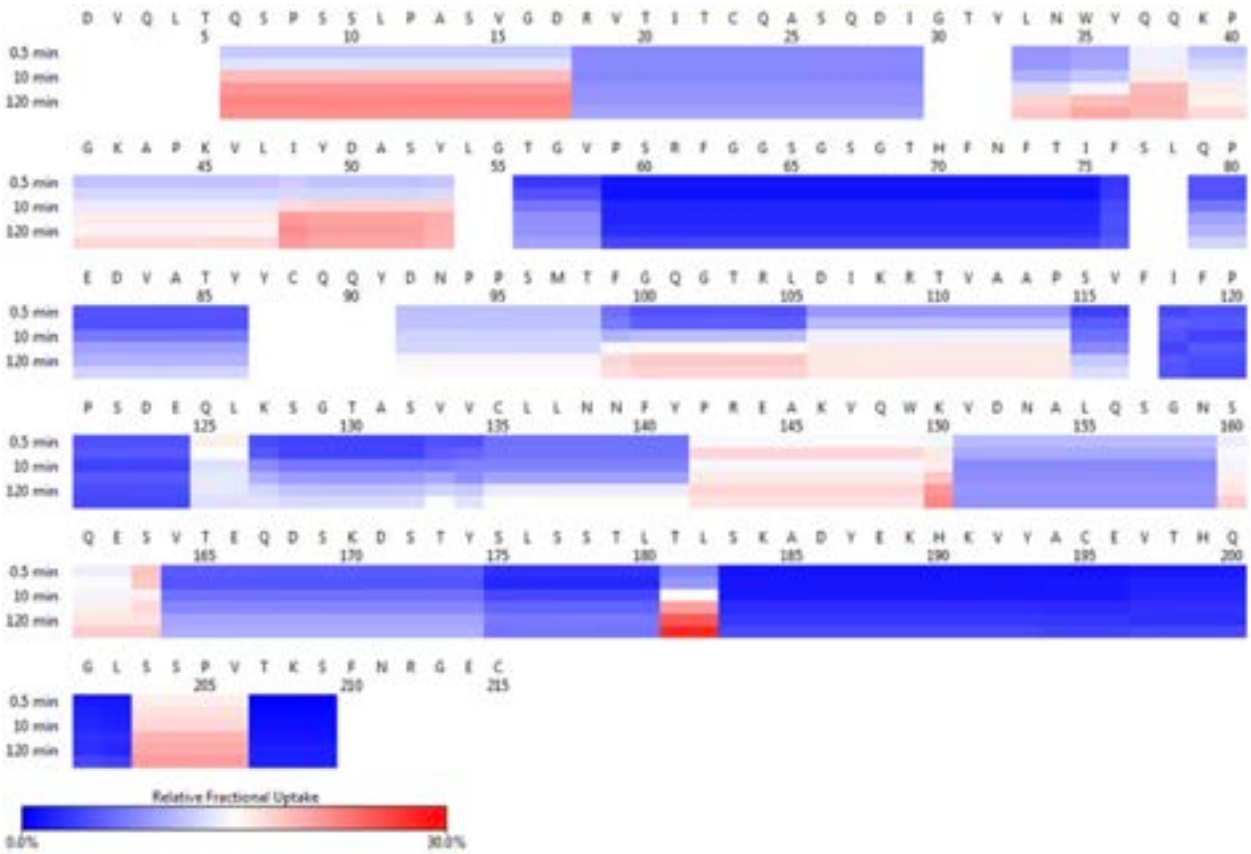

Figure S22. Heat map, related to Figure 5 and STAR methods. Heat map showing deuterium uptake by different peptides of glycosylated AC-LC31 in a gradient of blue-to-white-to-red for less to higher uptakes.

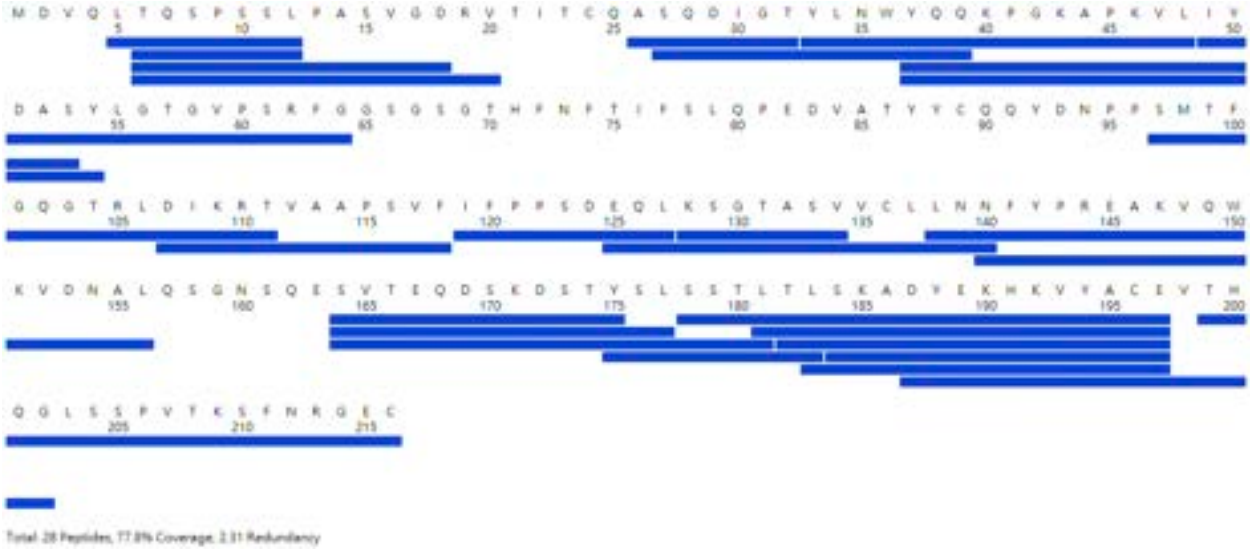

Figure S23. Coverage map, related to Figure 5 and STAR methods. Coverage map of common peptides between unglycosylated and glycosylated AC-LC31. The total number of

peptides is 28, with a coverage of 77.8 and redundancy of 2.31. The average length of all peptides is 12.6.

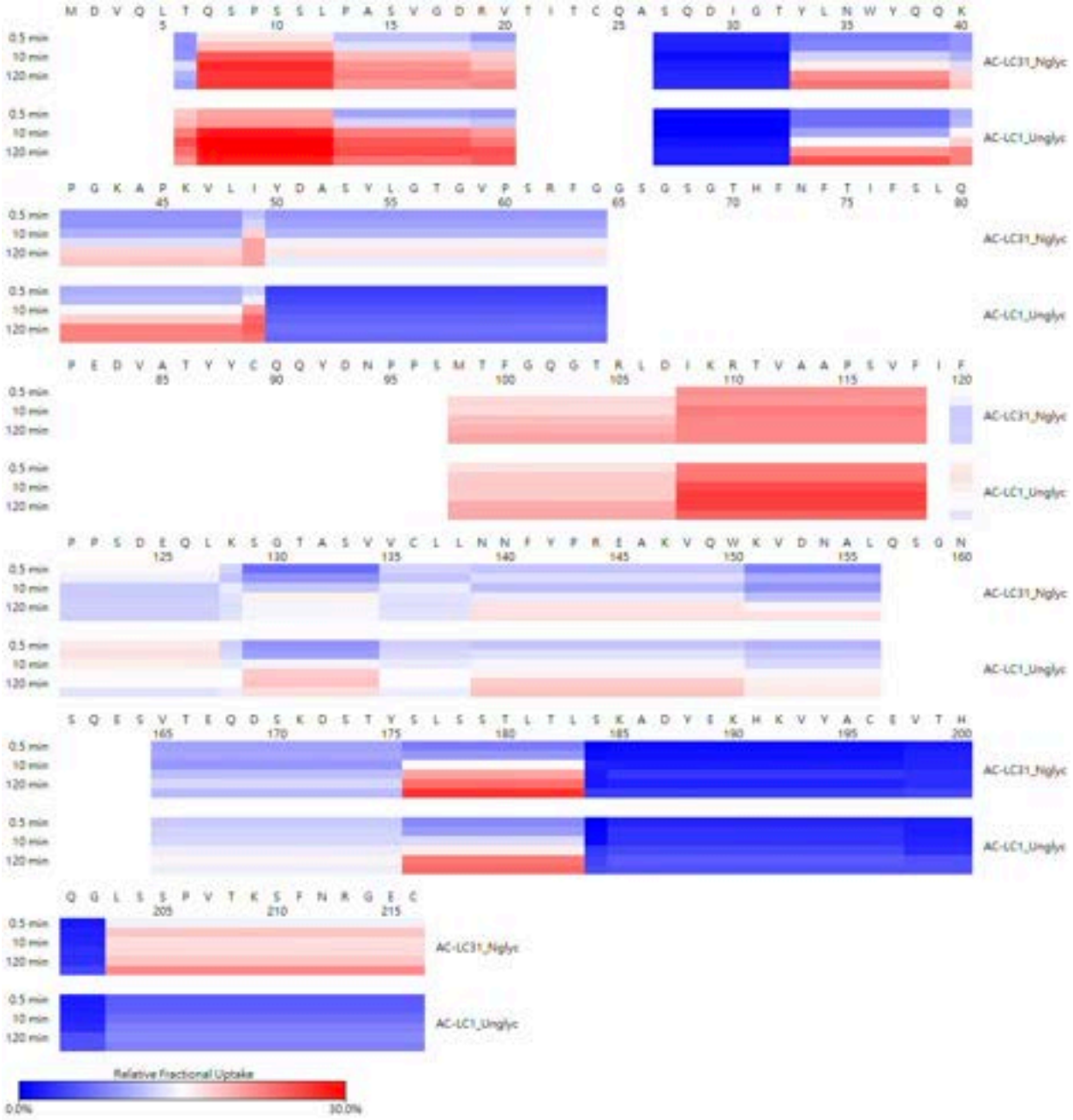

Figure S24. Heat map, related to Figure 5 and STAR methods. Heat map showing deuterium uptake by common peptides between unglycosylated and glycosylated AC-LC31.

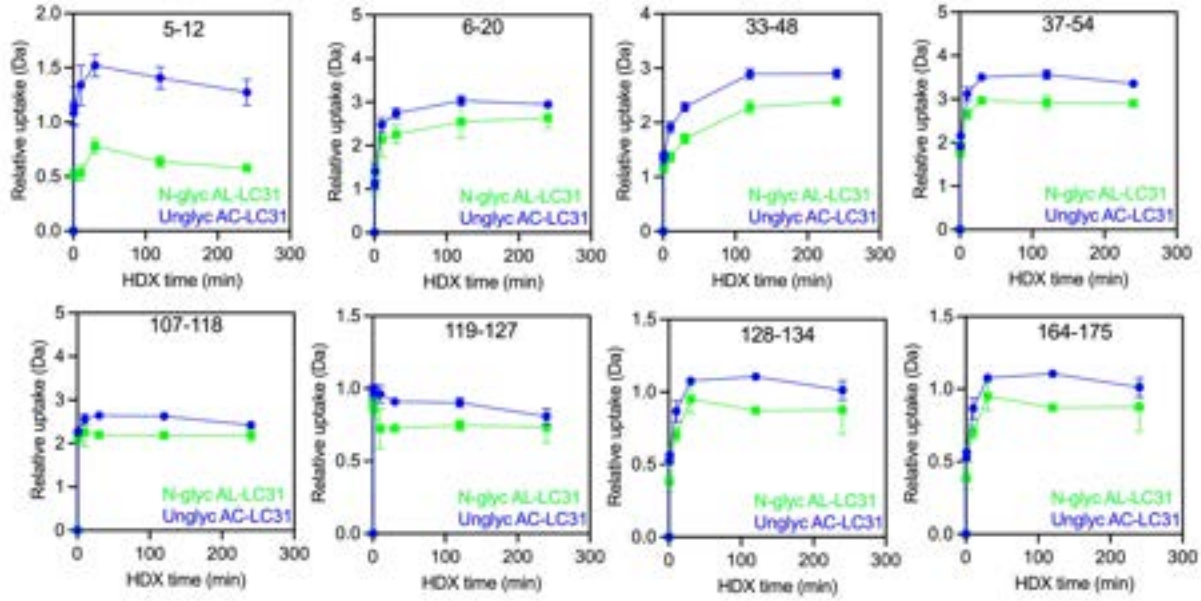

Figure S25. HDX-uptake kinetics plots obtained from Dynmax, related to Figure 5. HDX-uptake kinetics of relative deuterium uptake of the selected common peptides between N-glyc AC-LC31 (green) and unglyc AC-LC31 (blue). The error bars represent the standard deviation with respect to each exchange.

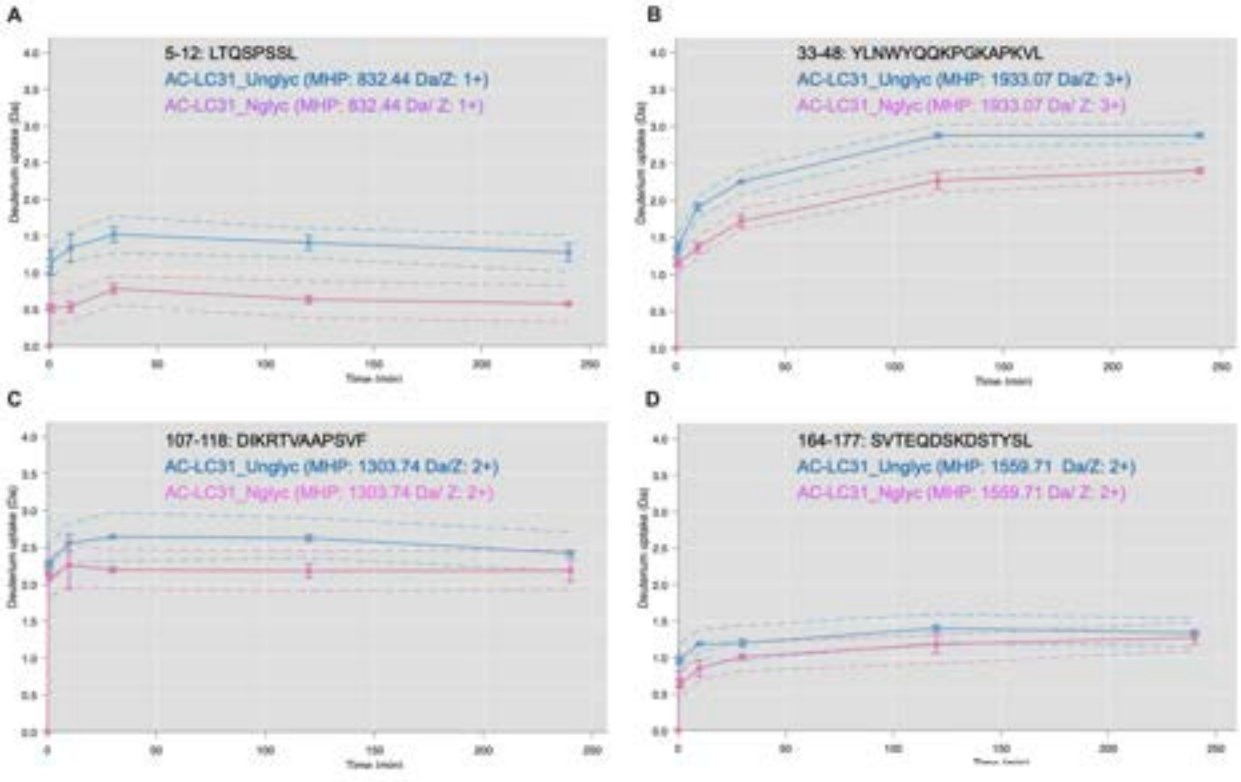

Figure S26. HDX-uptake kinetics plots obtained from Deutero 2, related to Figure 5. HDX-uptake kinetics of relative deuterium uptake of the selected common peptides between N-glyc

AC-LC31 (pink) and unglyc AC-LC31 (blue) by Deuteros 2.0 software. The error bars represent the standard deviation with respect to each exchange.

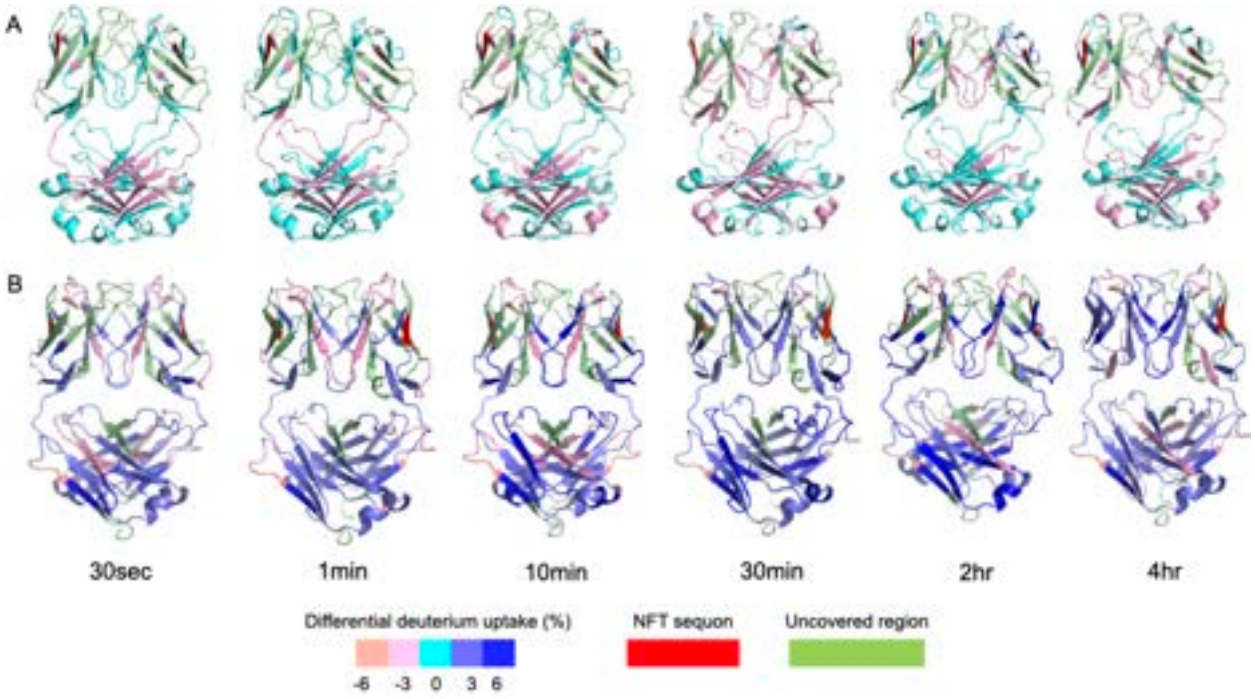

Figure S27. Structural mapping of differential deuterium uptakes between unglycosylated and N-glycosylated LCs, related to Figure 5. Structural mapping of differential deuterium uptake obtained after subtracting the deuterium uptake by unglycosylated proteins from their N-glycosylated counterparts. Negative value of deuterium uptake means higher uptake of deuterium by N-glycosylated proteins, and a positive value of deuterium uptake means lower uptake by N-glycosylated proteins. Zero means no difference in uptake (light blue). A) Structural mapping of differential deuterium exchange between unglycosylated and N-glycosylated AC-LC1 at different time points of 0.5 to 240 min. The N-glycosylated AC-LC1 exhibited a similar exchange to its unglycosylated counterpart, indicating similar dynamics for both. (B) Structural mapping of differential deuterium uptake between unglycosylated and N-glycosylated AC-LC31. The dark blue color indicates a lower uptake by glycosylated AC-LC31 and, therefore, less dynamic than its unglycosylated counterpart. NFT sequon is coloured in red. The uncovered region is shown in pale green.

CELL PRESS DECLARATION OF INTERESTS POLICY

Transparency is essential for a reader's trust in the scientific process and for the credibility of published articles. At Cell Press, we feel that disclosure of competing interests is a critical aspect of transparency. Therefore, we require a "declaration of interests" section in which all authors disclose any financial or other interests related to the submitted work that (1) could affect or have the perception of affecting the author's objectivity or (2) could influence or have the perception of influencing the content of the article.

What types of articles does this apply to?

We require that you disclose competing interests for all submitted content by completing and submitting the form below. We also require that you include a "declaration of interests" section in the text of all articles even if there are no interests to declare.

What should I disclose?

We require that you and all authors disclose any personal financial interests (e.g., stocks or shares in companies with interests related to the submitted work or consulting fees from companies that could have interests related to the work), professional affiliations, advisory positions, board memberships (including membership on a journal's advisory board when publishing in that journal), or patent applications and/or registrations that are related to the subject matter of the contribution. As a guideline, you need to declare an interest for (1) any affiliation associated with a payment or financial benefit exceeding $10,000 p.a. or 5% ownership of a company or (2) research funding by a company with related interests. You do not need to disclose diversified mutual funds, 401ks, or investment trusts.

Authors should also disclose relevant financial interests of immediate family members. Cell Press uses the Public Health Service definition of "immediate family member," which includes spouse and dependent children.

Where do I declare competing interests?

Competing interests should be disclosed on this form as well as in a "declaration of interests" section in the manuscript. This section should include financial or other competing interests as well as affiliations that are not included in the author list. Examples of "declaration of interests" language include:

> "AUTHOR is an employee and shareholder of COMPANY."
> "AUTHOR is a founder of COMPANY and a member of its scientific advisory board."

NOTE: Primary affiliations should be included with the author list and do not need to be included in the "declaration of interests" section. Funding sources should be included in the "acknowledgments" section and also do not need to be included in the "declaration of interests" section. (A small number of front-matter article types do not include an "acknowledgments" section. For these articles, reporting of funding sources is not required.)

What if there are no competing interests to declare?

If you have no competing interests to declare, please note that in the "declaration of interests" section with the following wording:

> "The authors declare no competing interests."

CELL PRESS DECLARATION OF INTERESTS FORM

If submitting materials via Editorial Manager, please complete this form and upload with your initial submission. Otherwise, please email as an attachment to the editor handling your manuscript.

Please complete each section of the form and insert any necessary "declaration of interests" statement in the text box at the end of the form. A matching statement should be included in a "declaration of interests" section in the manuscript.

Institutional affiliations

We require that you list the current institutional affiliations of all authors, including academic, corporate, and industrial, on the title page of the manuscript. ***Please select one of the following:***

☒ All affiliations are listed on the title page of the manuscript.

☐ I or other authors have additional affiliations that we have noted in the "declaration of interests" section of the manuscript and on this form below.

Funding sources

We require that you disclose all funding sources for the research described in this work. ***Please confirm the following:***

☒ All funding sources for this study are listed in the "acknowledgments" section of the manuscript.*

*A small number of front-matter article types do not include an "acknowledgments" section. For these, reporting funding sources is not required.

Competing financial interests

We require that authors disclose any financial interests and any such interests of immediate family members, including financial holdings, professional affiliations, advisory positions, board memberships, receipt of consulting fees, etc., that:

(1) could affect or have the perception of affecting the author's objectivity, *or*
(2) could influence or have the perception of influencing the content of the article.

Please select one of the following:

☒ We, the authors and our immediate family members, have no financial interests to declare.

☐ We, the authors, have noted any financial interests in the "declaration of interests" section of the manuscript and on this form below, and we have noted interests of our immediate family members.

Advisory/management and consulting positions

We require that authors disclose any position, be it a member of a board or advisory committee or a paid consultant, that they have been involved with that is related to this study. We also require that members of our journal advisory boards disclose their position when publishing in that journal. ***Please select one of the following:***

☒ We, the authors and our immediate family members, have no positions to declare and are not members of the journal's advisory board.

☐ The authors and/or their immediate family members have management/advisory or consulting relationships noted in the "declaration of interests" section of the manuscript and on this form below.

Patents

We require that you disclose any patent applications and/or registrations related to this work by any of the authors or their institutions. ***Please select one of the following:***

☒ We, the authors and our immediate family members, have no related patent applications or registrations to declare.

☐ We, the authors, have a patent application and/or registration related to this work, which is noted in the "declaration of interests" section of the manuscript and on this form below, and we have noted the patents of immediate family members.

Please insert any "declaration of interests" statements in this space. This exact text should also be included in the "declaration of interests" section of the manuscript. If no authors have a competing interest, please insert the text, "The authors declare no competing interests."

The authors declare no competing interests.

☒ **On behalf of all authors, I declare that I have disclosed all competing interests related to this work. If any exist, they have been included in the "declaration of interests" section of the manuscript.**